Journal of Medicinal Chemistry

Article

pubs.acs.org/jmc

Discovery of 5-Substituted Pyrrolo[2,3-*d*]pyrimidine Antifolates as Dual-Acting Inhibitors of Glycinamide Ribonucleotide Formyltransferase and 5-Aminoimidazole-4-carboxamide Ribonucleotide Formyltransferase in De Novo Purine Nucleotide Biosynthesis: Implications of Inhibiting 5-Aminoimidazole-4-carboxamide Ribonucleotide Formyltransferase to AMPK Activation and Antitumor Activity

Shermaine Mitchell-Ryan,[†,⊥] Yiqiang Wang,[‡,⊥,#] Sudhir Raghavan,[‡] Manasa Punaha Ravindra,[‡] Eric Hales,[§,†] Steven Orr,[§,†] Christina Cherian,[§,†] Zhanjun Hou,[§,†] Larry H. Matherly,*[,†,§,∥,⊥] and Aleem Gangjee*[,‡,⊥]

[†]Department of Oncology, Wayne State University School of Medicine, Detroit, Michigan 48201, United States

[‡]Division of Medicinal Chemistry, Graduate School of Pharmaceutical Sciences, Duquesne University, 600 Forbes Avenue, Pittsburgh, Pennsylvania 15282, United States

[§]Molecular Therapeutics Program, Barbara Ann Karmanos Cancer Institute, 110 East Warren Ave, Detroit, Michigan 48201, United States

[∥]Department of Pharmacology, Wayne State University School of Medicine, Detroit, Michigan 48201, United States

Supporting Information

ABSTRACT: We synthesized 5-substituted pyrrolo[2,3-*d*]pyrimidine antifolates (compounds **5**−**10**) with one-to-six bridge carbons and a benozyl ring in the side chain as antitumor agents. Compound **8** with a 4-carbon bridge was the most active analogue and potently inhibited proliferation of folate receptor (FR) α-expressing Chinese hamster ovary and KB human tumor cells. Growth inhibition was reversed completely or in part by excess folic acid, indicating that FRα is involved in cellular uptake, and resulted in S-phase accumulation and apoptosis. Antiproliferative effects of compound **8** toward KB cells were protected by excess adenosine but not thymidine, establishing de novo purine nucleotide biosynthesis as the targeted pathway. However, 5-aminoimidazole-4-carboxamide (AICA) protection was incomplete, suggesting inhibition of both AICA ribonucleotide formyltransferase (AICARFTase) and glycinamide ribonucleotide formyltransferase (GARFTase). Inhibition of GARFTase and AICARFTase by compound **8** was confirmed by cellular metabolic assays and resulted in ATP pool depletion. To our knowledge, this is the first example of an antifolate that acts as a dual inhibitor of GARFTase and AICARFTase as its principal mechanism of action.

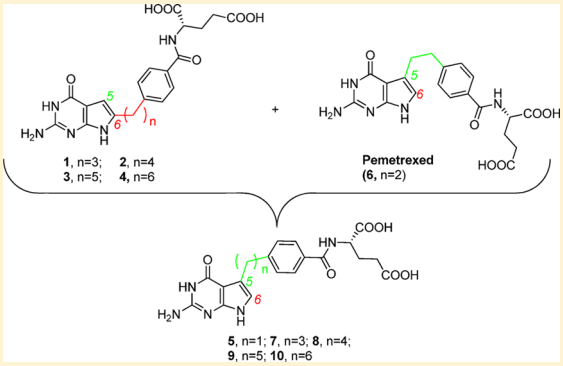

INTRODUCTION

The antifolates are a class of antiproliferatives widely recognized for their inhibition of folate metabolism.[1,2] Major antifolate enzyme targets include thymidylate synthase (TS) and dihydrofolate reductase (DHFR). Inhibition of these enzymes suppresses de novo nucleotide biosynthesis, resulting in an imbalance of purine and pyrimidine precursors and rendering cells incapable of undergoing accurate DNA replication, ultimately resulting in cell death. Clinically relevant TS (e.g., pemetrexed, PMX) and DHFR (e.g., methotrexate (MTX) and pralatrexate) inhibitors (Figure 1) continue to play important roles in treating hematologic malignancies and solid tumors.[1,2]

Antifolates targeting de novo purine nucleotide biosynthesis were also described and include lometrexol ((6*R*)5,10-dideazatetrahydrofolate, LMTX) (Figure 1), (2*S*)-2-((5-(2-((6*R*)-2-amino-4-oxo-5,6,7,8-tetrahydro-1*H*-pyrido[2,3-*d*]-pyrimidin-6-yl)ethyl)thiophene-2-carbonyl)amino)-pentanedioic acid (LY309887),[3,4] and (2*S*)-2-((5-(2-((6*S*)-2-amino-4-oxo-1,6,7,8-tetrahydropyrimido[5,4-bate][1,4]thiazin-6-yl)ethyl)thiophene-2-carbonyl)amino)pentanedioic acid (AG2034).[5] All of these drugs inhibit the first folate-dependent step in purine nucleotide biosynthesis, catalyzed by β-

Received: August 28, 2013
Published: November 20, 2013

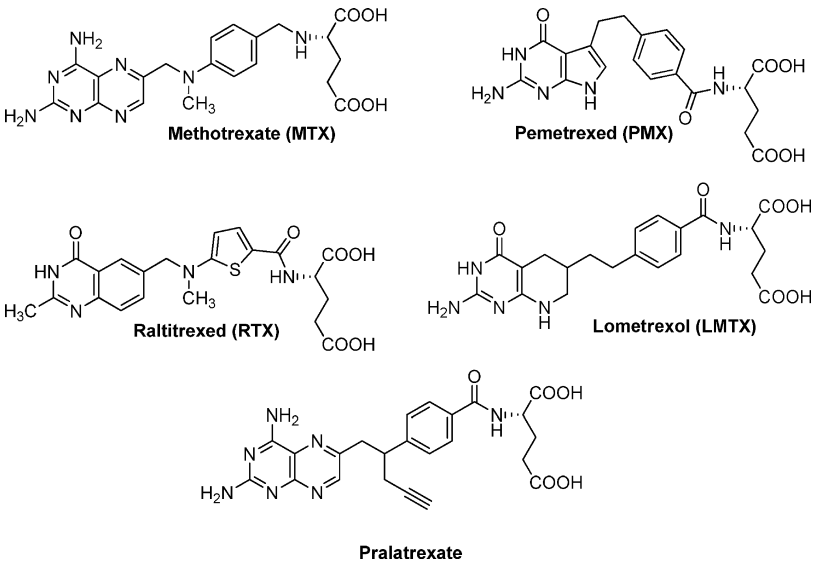

Figure 1. Structures of classical antifolates including methotrexate (MTX), pemetrexed (PMX), raltitrexed (RTX), lometrexol (LMTX), and pralatrexate.

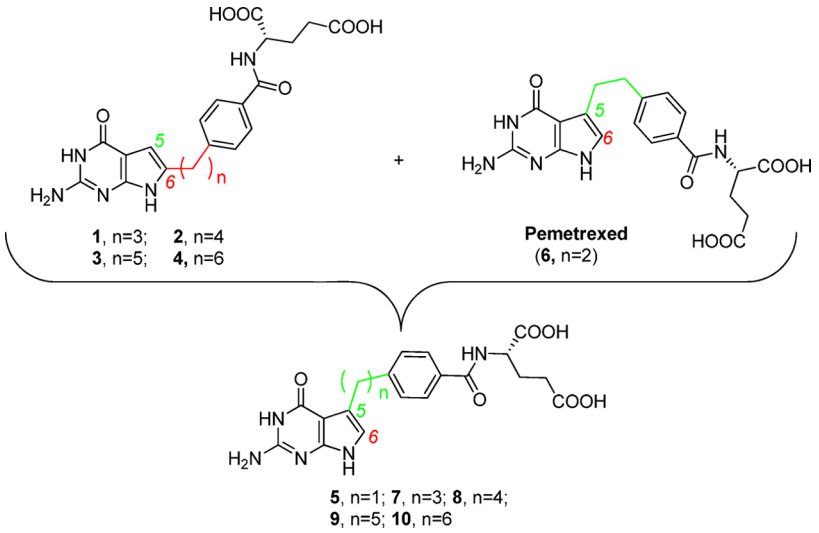

Figure 2. Design of 5-substituted pyrrolo[2,3-*d*]pyrimidines **5** and **7**−**10** (n = 1 or 3−6) based on structures of 6-substituted analogues **1**−**4** and pemetrexed.

glycinamide ribonucleotide (GAR) formyltranferase (GARFTase), and have progressed to clinical trials.[4,6,7] However, their toxicities were dose-limiting, most likely a consequence of their cellular uptake and metabolism to polyglutamates in normal tissues.

The reduced folate carrier (RFC) is one of three principal mechanisms of (anti)folate uptake into mammalian cells.[8] Cellular requirements for folate cofactors for DNA replication provide a plausible explanation for the high levels of RFC in most tumors. However, demands for folates, and consequently RFC, are also shared by normal tissues such that RFC may not be the optimal mechanism for tumor-selective uptake of cytotoxic folate analogues. Other cellular uptake mechanisms, notably, the proton-coupled folate transporter (PCFT) and folate receptors (FRs) α and β, are also expressed in tumors and show more restricted expression in normal tissues.[9] Furthermore, PCFT is a proton symporter such that in the acidic microenvironment generated by glycolytic tumors, membrane transport and selective tumor targeting by this mechanism is enhanced.[10,11] For FRα, the apical spatial orientation in normal epithelial tissues is often disrupted in tumors such that its basolateral membrane expression in tumors results in exposure to the circulation.[9] These features provide a compelling rationale for developing folate-based therapeutics that target PCFT and FRα for cancer therapy. Examples of FRα-targeted therapies include a monoclonal antibody, Farletuzumab (Morphotech),[12] a cytotoxic folate conjugate, Vintafolide (EC145; Endocyte),[13] and, ONX0801, a classical antifolate that is selectively transported into cells by FRs over RFC and inhibits de novo thymidylate biosynthesis.[14]

PMX is a 5-substituted pyrrolo[2,3-*d*]pyrimidine antifolate with a 2-carbon bridge linked to a *p*-aminobenzoyl glutamate. PMX is a good transport substrate for RFC and is among the best PCFT substrates,[8,10,11] yet it is a modest substrate for FRs.[15−19] We previously described 6-substituted pyrrolo[2,3-*d*]pyrimidine benzoyl antifolates related to PMX (compounds **1**−**4**) (Figure 2).[15,20] Whereas the 6-regioisomer of PMX was pharmacologically inert, the 3- and 4-bridge carbon analogues

dx.doi.org/10.1021/jm401328u | *J. Med. Chem.* 2013, 56, 10016−10032

Scheme 1

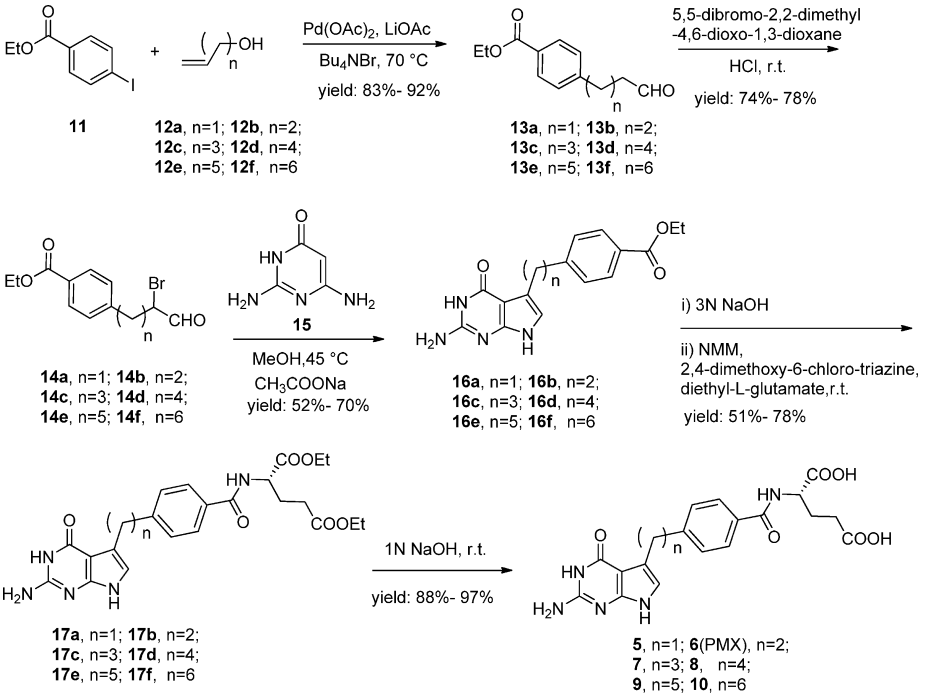

of this series (compounds **1** and **2**, respectively) were selectively transported by FRα and PCFT over RFC and were potently inhibitory toward FRα- and PCFT-expressing tumor cells.[15,20]

PMX was originally described as a multitargeted antifolate with a primary inhibition at TS and secondarily at GARFTase and DHFR.[21] However, recent studies suggested that although TS was the primary cellular target of PMX, 5-aminoimidazole-4-carboxamide (AICA) ribonucleotide (ZMP) formyltransferase (AICARFTase) could be a pharmacologically important target in the presence of excess thymidine (circumvents TS) at sufficiently high PMX concentrations.[22,23] Hence, in the presence of thymidine, inhibition of proliferation of CCRF-CEM leukemia cells and solid tumor cell lines was circumvented by hypoxanthine but only partially by AICA.[22,23] Furthermore, PMX resulted in marked accumulations of ZMP, the AICARFTase substrate. By contrast, the 6-substituted pyrrolo[2,3-*d*]pyrimidine analogues **1** and **2** are exclusively GARFTase inhibitors whose inhibitory effects are completely circumvented by AICA.[15,20]

The accumulation of ZMP in PMX-treated cells is intriguing because ZMP is an AMP mimetic that activates AMP-activated protein kinase (AMPK).[24] AMPK negatively regulates mTOR, a critical prosurvival pathway that is activated in many tumor cells along with PI3K/AKT, secondary to loss or mutation of PTEN.[25−27] This may provide a possible explanation for the growth inhibitory effects of PMX in the presence of thymidine, as purine nucleotides are not depleted.[22,23] However, this has not been directly tested because no AICARFTase-targeted drugs without TS inhibition have been described.

In this article, we synthesized and systematically characterized the in vitro antiproliferative activities and cellular mechanisms of novel 5-substituted pyrrolo[2,3-*d*]pyrimidine antifolates (including PMX) with a benzoyl ring in the side chain and one-to-six bridge carbons (compounds **5**−**10**) closely related to 6-substituted pyrrolo[2,3-*d*]pyrimidine analogues **1**−**4**[15,20] (Figure 2). We reasoned that the 5-substituted analogues might inhibit AICARFTase, analogous to PMX, albeit without TS inhibition. Furthermore, if this was accompanied by FRα and/or PCFT transport selectivity over RFC, then this would be especially appealing for targeting tumors that express high levels of these systems.

We describe herein the impact of these structural modifications on (i) transporter specificity and (ii) the targeted pathway (TS versus de novo purine nucleotide biosynthesis), including (iii) the extent of cellular GARFTase and AICARFTase inhibition. Our results document an emerging structure−activity relationship (SAR) for the pyrrolo[2,3-*d*]pyrimidine antifolates, accompanying translocation of the 6-pyrrolo[2,3-*d*]pyrimidine substituent to the regio 5-position, including sustained FRα cellular uptake, accompanying restoration of RFC and loss of PCFT transport activities. The 4-carbon bridge analogue of this series (compound **8**) is unique in that it shows dual inhibition of both AICARFTase and GARFTase exclusive of TS in tumor cells, resulting in depletion of purine nucleotides. Finally, our results directly examine the possibility of whether AMPK activation secondary to AICARFTase inhibition contributes to decreased proliferation of KB human tumor cells.

■ CHEMISTRY

Compounds **5**−**10** (n = 1−6) were obtained from a modified synthesis of PMX[28,29] using an α-bromo aldehyde condensation with 2,6-diamino-4-oxo-pyrimidine **15** as the key step (Scheme 1). Thus, a Heck coupling reaction[30] of aryl iodide **11** with commercially available unsaturated alcohols **12a**−**f** in DMF at 70 °C affords the unsaturated, coupled alcohols that rearrange to the vinyl alcohols and tautomerise to afford aldehydes **13a**−**f** (yields: 83−92%), as reported by Larock et al.[30] α-Bromonation of **13a**−**f** with 5,5-dibromo-2,2-dimethyl-4,6-dioxo-1,3-dioxane[31] at room temperature afforded corresponding α-bromo aldehydes **14a**−**f** (yields: 74−78%). 5-Substituted pyrrolo[2,3-*d*]pyrimidines **16a**−**f** were synthesized by con-

dx.doi.org/10.1021/jm401328u | J. Med. Chem. 2013, 56, 10016−10032

Table 1. IC_{50} Values (nM) for 5- and 6-Substituted Pyrrrolo[2,3-*d*]pyrimidine Antifolates and Classical Antifolates in RFC-, PCFT-, and FR-Expressing Cell Lines[a]

		hRFC		hFRα		hPCFT		hRFC/FRα/hPCFT		
compound	structure	PC43-10	R2	RT16	RT16 (+FA)	R2/hPCFT4	R2(VC)	KB	KB (+FA)	KB (+Thd/Ade/AICA)
1	6-pyrrole/3C	648.6(38.1)	>1000	4.1(1.6)	>1000	23.0(3.3)	>1000	1.7(0.4)	>1000	Ade/AICA
2	6-pyrrole/4C	>1000	>1000	6.3(1.6)	>1000	213 (28)	>1000	1.9(0.7)	>1000	Ade/AICA
3	6-pyrrole/5C	>1000	>1000	54(21)	>1000	>1000	>1000	13(7.2)	>1000	Ade/AICA
4	6-pyrrole/6C	>1000	>1000	162(18)	>1000	>1000	>1000	23(12)	>1000	Ade/AICA
5	5-pyrrole/1C	>1000	>1000	>1000	>1000	>1000	>1000	>1000	>1000	
6 (PMX)	5-pyrrole/2C	30.6 (6.2)	>1000	18.2(3.8)	>1000	22.3(8.6)	>1000	9.94(3.11)	690 (310)	Thd/Ade
7	5-pyrrole/3C	68.8(21.2)	>1000	72.0(27.1)	>1000	329(61)	>1000	49.5(13.2)	533(233)	Ade
8	5-pyrrole/4C	56.6(5.8)	>1000	8.6(2.1)	>1000	840(90)	>1000	12.7(5.4)	700 (300)	Ade
9	5-pyrrole/5C	196.4 (55.0)	>1000	33.5(2.5)	>1000	>1000	>1000	17.3(8.9)	898(102)	Ade/AICA
10	5-pyrrole/6C	>1000	>1000	>1000	>1000	>1000	>1000	>1000	>1000	
MTX		12(1.1)	216(8.7)	114(31)	461(62)	120.5(16.8)	>1000	6.0(0.6)	20(2.4)	Thd/Ade
RTX		6.3(1.3)	>1000	15(5)	>1000	99.5(11.4)	>1000	5.9(2.2)	22(5)	Thd
LMTX		12(2.3)	>1000	12(8)	188(41)	38.0(5.3)	>1000	1.2(0.6)	31(7)	Ade/AICA

[a]Growth inhibition assays were performed for CHO sublines engineered to express human RFC (PC43-10), FRα (RT16), or PCFT (R2/PCFT4) for comparison with transporter-null (R2 and R2(VC)) CHO cells and for the KB human tumor sublines (expressing RFC, FRα, and PCFT). For the FRα experiments, growth inhibition assays were performed in the presence and absence of 200 nM folic acid (FA). The data shown are mean values from 3 to 10 experiments (± standard errors in parentheses). The results are presented as IC_{50} values corresponding to the concentrations that inhibit growth by 50% relative to cells incubated without drug. Data for MTX, RTX, LMTX, and compounds **1**, **2**, **3**, and **4** were previously published[15] (structures for compounds **1**–**10** are in Figure 2). For KB cells, data are shown for the protective effects of nucleoside additions, including adenosine (60 μM) or thymidine (10 μM), or 5-aminoimidazole-4-carboxamide (320 μM). Examples of these data are in Figure 5. For 5- and 6-pyrrolo-2,3-*d*]pyrimidine compounds **1**–**10**, the structural motifs are noted (i.e., the pyrrole substitution/bridge length). Experimental details are provided in the Experimental Section. Abbreviations: Ade, adenosine; AICA, 5-aminoimidazole-4-carboxamide; and Thd, thymidine.

densation of **14a**–**f** with **15** at 45 °C in the presence of sodium acetate (yields: 52–70%). Subsequent hydrolysis with 3 N NaOH followed by coupling with diethyl L-glutamate using *N*-methyl morpholine and 2,4-dimethoxy-6-chlorotriazine as the activating agents afforded diesters **17a**–**f** (yields: 51–78% over two steps). Final saponification of the diesters with 1 N NaOH provided target compounds **5**–**10** (yields: 88–97%).

BIOLOGICAL EVALUATION

Transporter Selectivity for Inhibition of Cell Proliferation by 5- and 6-Substituted Pyrrolo[2,3-*d*]pyrimidine Regioisomers. Our initial goal was to define better the SARs for membrane transport of pyrrolo[2,3-*d*]pyrimidine antifolates relating to the impact of 5- versus 6-substitutions on the pyrrole ring, which is based on the established antitumor activities of 6-substituted pyrrolo[2,3-*d*]pyrimidine-substituted compounds **1** and **2** with 3- and 4-bridge carbons, respectively,[15,20] and the preclinical and clinical efficacy of PMX,[21] a 5-substituted pyrrolo[2,3-*d*]pyrimidine with a 2-carbon bridge (Figure 2). In our previous studies,[15,20] compounds **1** and **2** were efficiently internalized by tumor cells via FRα and PCFT but not by RFC, whereas PMX was a substrate by all three systems.[15−20]

Transporter specificities are exemplified by patterns of inhibition of cell proliferation toward isogenic Chinese hamster ovary (CHO) cell models engineered to express human RFC (PC43-10), PCFT (R2/PCFT4), or FRα (RT16)[15−19] treated with compounds **1**–**4** (Table 1). The results are compared to those for RFC-, PCFT-, and FR-null MTXRIIOua^{R}2-4 (R2) CHO cells. As previously reported,[15,20] compounds **1**–**4** inhibited proliferation of FRα-expressing RT16 and R2/PCFT4 cells in the following order of potency: **1** > **2** > **3** > **4**. However, compounds **1**–**4** were largely inactive toward RFC-expressing PC43-10 and R2 cells. Analogous results were obtained with KB nasopharyngeal carcinoma cells that express elevated FRα along with modest levels of RFC and PCFT.[16] The antiproliferative effects of compounds **1**–**4** toward the FRα-expressing cell lines were abolished in the presence of excess (200 nM) folic acid, establishing that the cellular uptake of these analogues is mediated primarily via FRα[15] (Table 1).

5-Substituted pyrrolo[2,3-*d*]pyrimidine analogues with a side-chain benzoyl group (analogues of compounds **1**–**4**) and bridge lengths from one-to-six carbons (compounds **5**–**10**) were synthesized (Scheme 1) and tested for their antiproliferative activities toward the CHO and human tumor cell line models (Table 1). The 5-pyrrolo[2,3-*d*]pyrimidine analogue with a 2-carbon bridge (compound **6**) is PMX. 5-Pyrrole substitution restored RFC-directed antiproliferative activity, as reflected in the dramatically increased antiproliferative effects of this series toward PC43-10 cells compared to RFC-, PCFT-, and FR-null R2 cells in the following order of potency (numbers of bridge carbons are noted in parentheses): **6** (2C) > **8** (4C) ∼**7** (3C) > **9** (5C) ≫ **5** (1C) ∼**10** (6C). For PCFT-expressing R2/PCFT4 CHO cells and with the exception of compound **6**, antiproliferative effects for the 5-substituted analogues were attenuated compared to the 6-substituted analogues (e.g., for direct comparisons between paired 5- and 6-substituted analogues, compare IC_{50}'s for compounds **7**–**10** to **1**–**4**, respectively, in Table 1).

With the FRα-expressing sublines, potencies were also reduced for the 5-substituted compounds compared to the 6-substituted analogues. These differences ranged from slight (compare **2** to **8** and **3** to **9**) to substantial (compare **1** to **7**) (Table 1). For both series, the 6-carbon bridge analogues (compounds **4** and **10**) were inactive. In contrast to the results for PCFT- and RFC-expressing cells, the impacts of bridge length were distinctly different, with antiproliferative activities toward FRα-expressing RT16 CHO cells in rank order **8** (4C) > **6** (2C) > **9** (5C) > **7** (3C) ≫ **5** (1C) ∼ **10** (6C). An analogous pattern of sensitivities was obtained with KB human tumor cells, and for both the KB and RT16 cell lines, inhibitory

dx.doi.org/10.1021/jm401328u | J. Med. Chem. 2013, 56, 10016−10032

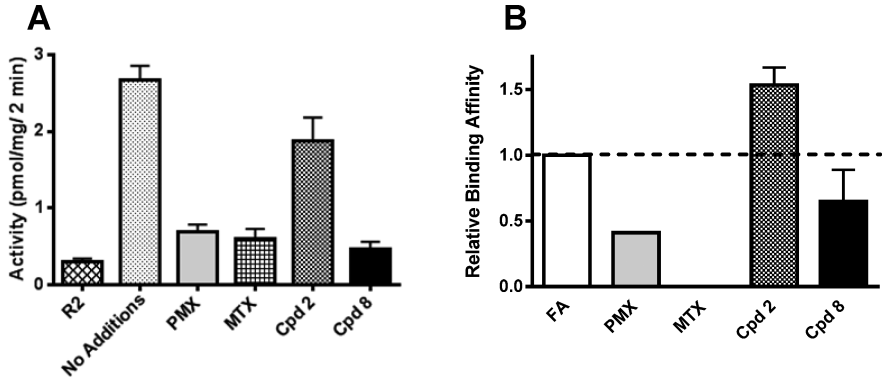

Figure 3. Inhibition of RFC-mediated transport and relative FRα-binding affinities by 6- (compound **2**) and 5-substituted (compound **8**) pyrrolo[2,3-*d*]pyrimidine antifolates. (A) To determine if novel antifolates were able to bind human RFC and inhibit transport of [^{3}H]MTX, reflecting transport of the novel analogues by this mechanism, we used PC43-10 CHO cells ectopically expressing human RFC but not FRs or PCFT. Uptake of 0.5 μM [^{3}H]MTX was measured in the absence or presence of 10 μM nonradioactive inhibitors, including compound (Cpd) **2** or **8** or the classical agents PMX and MTX. Transport results are compared to those for RFC-null R2 cells. (B) To assess the relative binding affinities of the novel antifolates to FRα, we performed direct competitive binding assays using [^{3}H]folic acid (FA) in the FRα-engineered CHO cell line, RT16, in the presence or absence of various concentrations of unlabeled pyrrolo[2,3-*d*]pyrimidine compounds **2** or **8** or folic acid, PMX, or MTX.[15]

effects were substantially reversed by 200 nM folic acid, confirming FRα as an important uptake mechanism for these compounds.

To complement the results showing antiproliferative effects of the most potent 5-substituted analogue **8** toward PC43-10 CHO cells expressing human RFC, we measured competitive inhibitions of [^{3}H]MTX (0.5 μM) transport in this model (Figure 3A). MTX is a well-characterized surrogate substrate for RFC, and the extent of [^{3}H]MTX transport inhibition by competitive unlabeled (anti)folate ligands correlates with their membrane transport by RFC.[8] For our study, we compared inhibitory effects of 10 μM compound **8** to those for corresponding 6-substituted compound **2** as well as to PMX and MTX. Transporter-null R2 cells were used as a measure of the baseline [^{3}H]MTX uptake. Whereas **2** was a poor inhibitor of [^{3}H]MTX uptake (<25% inhibition), 10 μM compound **8** was a reasonably good inhibitor (>90% inhibition), with an inhibitory potency approximating that for PMX and a net transport only slightly greater than the very low levels recorded for R2 cells. Clearly, unlike the 6-substituted pyrrolo[2,3-*d*]pyrimidine analogues, the 5-substituted compounds lack specificity for FRα and/or PCFT over RFC.

Binding affinities for FRα are expressed relative to that for folic acid. For both the transport and binding assays, experimental details are provided in the Experimental Section, and the results are presented as mean values ± standard errors from three experiments.

Compound **8** showed antiproliferative effects toward FRα-expressing RT16 CHO cells and KB human tumor cells (Table 1). To demonstrate drug binding to FRα directly, a prerequisite of cellular uptake by this endocytotic mechanism, we used competitive binding assays of [^{3}H]folic acid with RT16 cells treated with unlabeled ligands that compete for FRα binding[15−19] (Figure 3B). Relative FRα binding affinities for the 5- (compound **8**) versus 6-substituted (compound **2**) analogues paralleled their antiproliferative activities. However, this correlation did not quite extend to PMX (compound **6**) or to MTX, indicating that multiple factors in addition to FRα binding affinities contribute to net growth inhibition of these FRα-expressing cells for the antifolates.

Inhibition of De Novo Purine Nucleotide Biosynthesis by Both 5- and 6-Pyrrolo[2,3-*d*]pyrimidine Compounds Leads to a Cytotoxic Response via Purine Nucleotide Depletion. De novo purine nucleotide biosynthesis includes 10 reactions by which phosphoribosyl pyrophosphate (PRPP) is converted into inosine monophosphate (IMP), the precursor of AMP and GMP (Figure 4). There are two folate-dependent enzymes in the pathway that are possible targets for folate-based therapies including GARFTase (catalyzes steps 2, 3, and 5) and AICARFTase (catalyzes steps 9 and 10). Previous studies established that GARFTase was the intracellular enzyme target for LMTX[3,32] as well as for compounds **1** and **2**.[15] For PMX, TS is the primary intracellular target, although modest inhibitions of GARFTase and DHFR were also reported.[21] Most recently, AICARFTase was implicated as a potentially important secondary enzyme target for PMX (in the presence of excess thymidine to circumvent TS inhibition) by nucleoside/AICA protection experiments and metabolic assays.[22,23]

To identify the targeted pathway for 6-substituted compounds **1** and **2**, we previously used nucleoside protection experiments with adenosine (60 μM) and thymidine (10 μM) to distinguish de novo purine nucleotide from thymidylate biosynthesis, respectively.[15−20,32] To identify further the likely folate-metabolizing-enzyme targets in purine nucleotide biosynthesis (GARFTase versus AICARFTase), cells were treated with the antifolates in the presence of AICA (320 μM), which is metabolized to AICA ribonucleotide (ZMP), the substrate for AICARFTase, thus bypassing the step catalyzed by GARFTase[15−20,32] (Figure 4).

We used this approach for KB cells treated with compounds **7**−**9**, with results compared to those for compound **2** and PMX (compound **6**) (Table 1; Figure 5 shows the nucleoside/AICA protection results for PMX and for compound **2** compared to those for compound **8**). With compound **2**, both adenosine and AICA were completely protective, establishing de novo purine biosynthesis and GARFTase as the principal cellular targets.[15,20] With PMX, thymidine, adenosine, and AICA were all partially protective, albeit to different extents. Combined thymidine and adenosine completely protected KB cells from the growth inhibitory effects of PMX (not shown; Table 1). The growth inhibitory effects of the 5-substituted compounds **7**−**9** with KB cells were unaffected by excess thymidine but were completely reversed in the presence of adenosine alone, indicating that de novo purine nucleotide

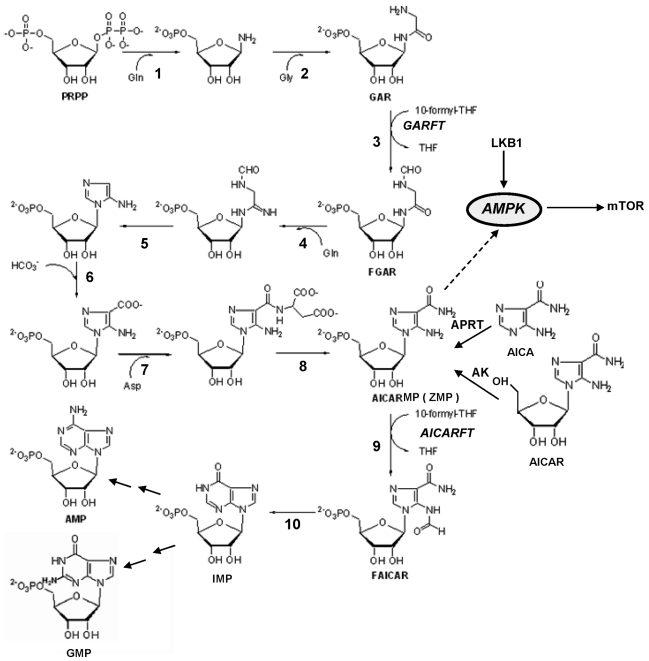

Figure 4. De novo purine nucleotide biosynthesis and relationship to AMPK. The de novo purine nucleotide biosynthetic pathway including the steps from phosphoribosyl pyrophosphate (PRPP) to IMP is shown. Reactions 1, 4, and 8 are catalyzed by glutamine phosphoribosylpyrophosphate amidotransferase, formylglycinamide ribonucleotide synthase, and adenylosuccinate lyase, respectively. Reactions 2, 3, and 5 are catalyzed by the trifunctional glycinamide ribonucleotide (GAR) formyltransferase (GARFTase), which contains GAR synthase (reaction 2), GAR formyltransferase (GARFTase; reaction 3), and 5-aminoimidazole ribonucleotide synthase (reaction **5**) activities. Reactions 6 and 7 are catalyzed by the bifunctional phosphoribosylaminoimidazole carboxylase/phosphoribosylaminoimidazole succinocarboxamide synthetase enzyme, which contains carboxyaminoimidazole ribonucleotide synthase (reaction 6) and 5-aminoimidazole-4-(*N*-succinylocarboxamide) ribonucleotide synthase (reaction 7) activities. Reactions 9 and 10 are catalyzed by 5-aminoimidazole-4-carboxamide ribonucleotide formyltransferase (AICARFTase)/IMP cyclohydrolase that catalyzes the last two steps in the pathway for de novo synthesis of IMP. Folate-dependent reactions (reactions 3 and 9), in which 10-formyl tetrahydrofolate (THF) serves as the one-carbon donor, are catalyzed by GARFTase and AICARFTase. 5-Aminoimidazole-4-carboxamide (AICA) and AICA ribonucleoside (AICAR) can be metabolized to 5-aminoimidazole-4-carboxamide ribonucleotide monophosphate (ZMP) by either adenine phosphoribosyl transferase (APRT) or adenosine kinase (AK), thus circumventing the reaction catalyzed by GARFTase. The activation of AMPK that results in inhibition of mTOR is also depicted. Abbreviations: AICAR, 5-aminoimidazole-4-carboxamide ribonucleoside; FGAR, formyl glycinamide ribonucleotide; FAICAR, formyl 5-aminoimidazole-4-carboxamide ribonucleotide; and MP, monophosphate.

synthesis was being targeted exclusively (rather than combined thymidylate and purine nucleotide synthesis as for PMX). Whereas AICA alone completely protected KB cells from the inhibitory effects of compound **9**, AICA alone was only partially protective with compounds **7** and **8**. Thus, inhibition of purine nucleotide biosynthesis by compounds **7** and **8** is likely a composite effect of dual inhibitions involving both GARFTase and AICARFTase. These results strongly imply that shifting the substituent from the 6- to the 5-position on the pyrrolo[2,3-*d*]pyrimidine ring system results in an altered inhibition of the targeted enzymes.

Decreased purine nucleotide biosynthesis resulting from inhibition of folate-dependent enzymes can be monitored by following changes in ATP pools, a surrogate measure of total purine nucleotides (Figure 6). KB tumor cells were treated for 24 h with novel 5-substituted analogue **8** or corresponding 6-subsituted regioisomer compound **2**. An additional incubation was performed with PMX. ATP pools were extracted and measured by an HPLC ion-pairing method.[20,33] In KB cells following a 24 h incubation, compound **8**, like **2**, potently depleted ATP pools (>90%), whereas PMX was less effective (~60% inhibition).

Inhibition of De Novo Purine Nucleotide Biosynthesis by Compound 8 Results in Cytotoxicity and Apoptosis. To confirm that depletion of purine nucleotides by compound **8** results in cytotoxicity toward KB cells, we performed colony-forming assays. In these experiments, KB tumor cells were treated with various concentrations (0.5−10 μM) for 48 h, then washed and plated without drug. Colonies were enumerated after 10 days (Figure 7A). Following drug exposure, the inhibitory effects of compound **8** were irreversible with complete loss of colony formation at the highest drug concentrations, thereby establishing compound **8** as cytotoxic.

Programmed cell death type I (mitochondrial pathway) requires ATP to form the death complex with cytochrome C and caspase 9 and to carry out other energy-requiring processes for enzymatic degradation and modification of cellular components.[34] Previous studies suggested that 6-substituted pyrrolo[2,3-*d*]pyrimidine antipurine antifolate **1** was capable of inducing apoptosis, albeit to a lower extent than for daunorubicin over 24 h.[15] Additional experiments were performed with KB cells treated with compound **8** to assess its effects on cell cycle progression and induction of apoptosis, with comparisons to PMX and compound **2**. Cells were exposed to 1 μM drugs for 48 or 96 h. Cultures were then divided, with one fraction fixed and stained with propidium iodide (PI) for flow cytometry analysis of cell cycle distribution (Figure 7B). An additional fraction was assayed for apoptosis by flow cytometry with annexin V-fluorescein isothiocyanate (FITC) /7-amino actinomycin D (AAD) staining (Figure 7C).

At 48 h, minimal effects on the cell cycle were observed except for PMX, which induced a G_1/G_o-phase arrest relative to the untreated (DMSO) control (Supporting Information, Figure 1S). At 96 h, all compounds tested increased the percentages of cells in S-phase (albeit to different extents) and reduced those in the G_1/G_o- and G_2/M-phases of the cell cycle (Figure 7B). A prominent increase in the sub-G_1 population at 96 h was also seen (Figure 7B; most notable for compounds **2** and **8**), indicating that apoptosis was induced. Annexin V-FITC/7-AAD staining was used to monitor the induction of apoptosis further. For compounds **2** and **8** as well as PMX, positive annexin V-FITC staining increased over time (results for 96 h are shown in Figure 7C; additional data at 48 h of drug exposure are shown in the Supporting Information, Figure 1S), with distinct increases in both early (annexin-V-FITC^{high}/7-AAD^{low}) and late (annexin-V-FITC^{high}/7-AAD^{high}) apoptotic fractions compared those for the untreated control (i.e., the fractions of cells in early apoptosis were 33.8 and 0.49% for compound **8**-treated and control cells, respectively, whereas the fractions in late apoptosis at 96 h were 26.7 and 2.1%, respectively). Nearly identical results were obtained with compound **2**, although for PMX the distribution between the

dx.doi.org/10.1021/jm401328u | J. Med. Chem. 2013, 56, 10016−10032

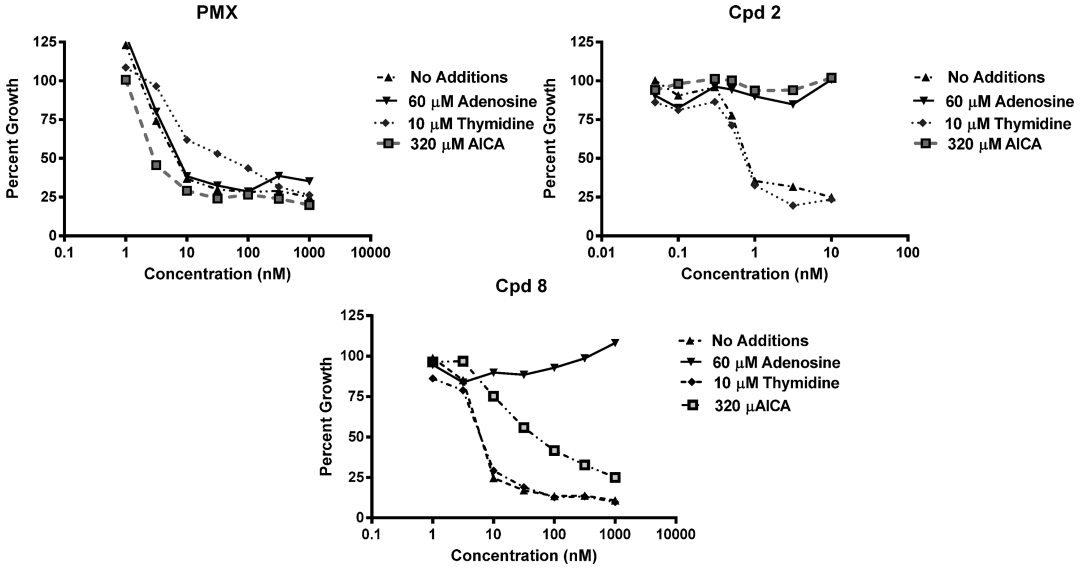

Figure 5. Cell proliferation assays with protection by nucleosides including thymidine and adenosine and by 5-aminoimidazole-4-carboxamide (AICA) to identify intracellular targets of PMX and compounds **2** and **8**. To identify the targeted pathways and the folate-dependent intracellular enzymes in KB cells treated with compound **8** (1−1000 nM), cell proliferation assays were performed in the presence of 10 μM thymidine, 60 μM adenosine, or 320 μM AICA. The results were normalized to those for untreated cells (no drug) and for compound **8**, the results are compared to those for PMX and compound **2**. Details are provided in the Experimental Section. The results shown are representative of triplicate experiments. Analogous protection experiments were performed for compounds **7** and **9**, and the results are summarized in Table 1 along with those for compounds **2** and **8**.

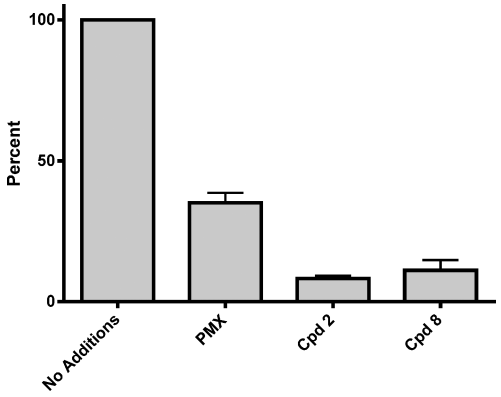

Figure 6. Compounds **2** and **8** deplete ATP pools in KB cells. KB cells were treated with 1 μM of novel 5- and 6-substituted pyrrolo[2,3-*d*]pyrimidine antifolates **2** and **8** or with PMX for 24 h. Nucleotides were extracted and analyzed by ion-pair HPLC. Details are in the Experimental Section. The results are presented as mean values ± standard errors.

early and late apoptotic fractions was somewhat different. Thus, 5- and 6-substituted pyrrolo[2,3-*d*]pyrimidines **2** and **8** can both induce apoptosis, resulting in cell death, in spite of depleted ATP pools.

Dual Inhibition of GARFTase and AICARFTase by 5-Substituted Pyrrolo[2,3-*d*]pyrimidine Antifolates and Downstream Effects of Accumulated ZMP on AMPK. Experiments were performed to measure cellular GARFTase activity in KB tumor cells treated with the 6- (compound **2**) and 5-substituted (compound **8** and PMX) pyrrolo[2,3-*d*]pyrimidines. For this purpose, we used an in situ activity assay for GARFTase that measures incorporation of [^{14}C]-glycine into [^{14}C]formyl GAR in the presence of azaserine over 16 h.[15−20,32]

Cells were treated with trichloroacetic acid (TCA), and, following deproteinization, acid-soluble metabolites were ether-extracted and fractionated by ion-exchange chromatography, permitting isolation and quantitation of [^{14}C]formyl GAR. Both 5- and 6-substituted analogues showed a dose-dependent decrease in the formation of [^{14}C]formyl GAR. However, compound **2** was more potent than either PMX or compound **8**, with an IC_{50} for this compound exceeding those for the 5-substituted compounds by 2- and 5-fold, respectively (Figure 8).

The antiproliferative effects of PMX independent of its impact on TS were previously attributed to its inhibition of AICARFTase in addition to GARFTase, as reflected in the incomplete protection by AICA in the presence of thymidine and the accumulation of the AICARFTase substrate ZMP in tumor cell lines treated with PMX, as measured by anion-exchange HPLC analysis.[22,23] ZMP accumulation showed both dose and time dependence for PMX and resulted in activation of AMPK (via its role as an AMP mimetic) and suppression of mTOR.

To validate the findings from our AICA protection experiments with compound **8** (Figure 6) and to explore whether AICARFTase is a bona fide target for this novel 5-substituted pyrrolo[2,3-*d*]pyrimidine, analogous experiments were performed to measure accumulation of ZMP in KB cells treated with 1 μM compound **8** as a measure of AICARFTase inhibition. Parallel assays in KB cells treated with PMX were performed. ZMP accumulated in the presence of PMX and compound **8** in a linear fashion for up to 48 h (not shown), with PMX showing approximately 2-fold increased levels over compound **8** (Figure 9A).

To verify the impact of ZMP accumulation on AMPK phosphorylation in KB cells treated with compound **8** or with PMX, western blot analysis was performed for total and phosphorylated AMPK in KB cells treated with these antifolates

dx.doi.org/10.1021/jm401328u | J. Med. Chem. 2013, 56, 10016−10032

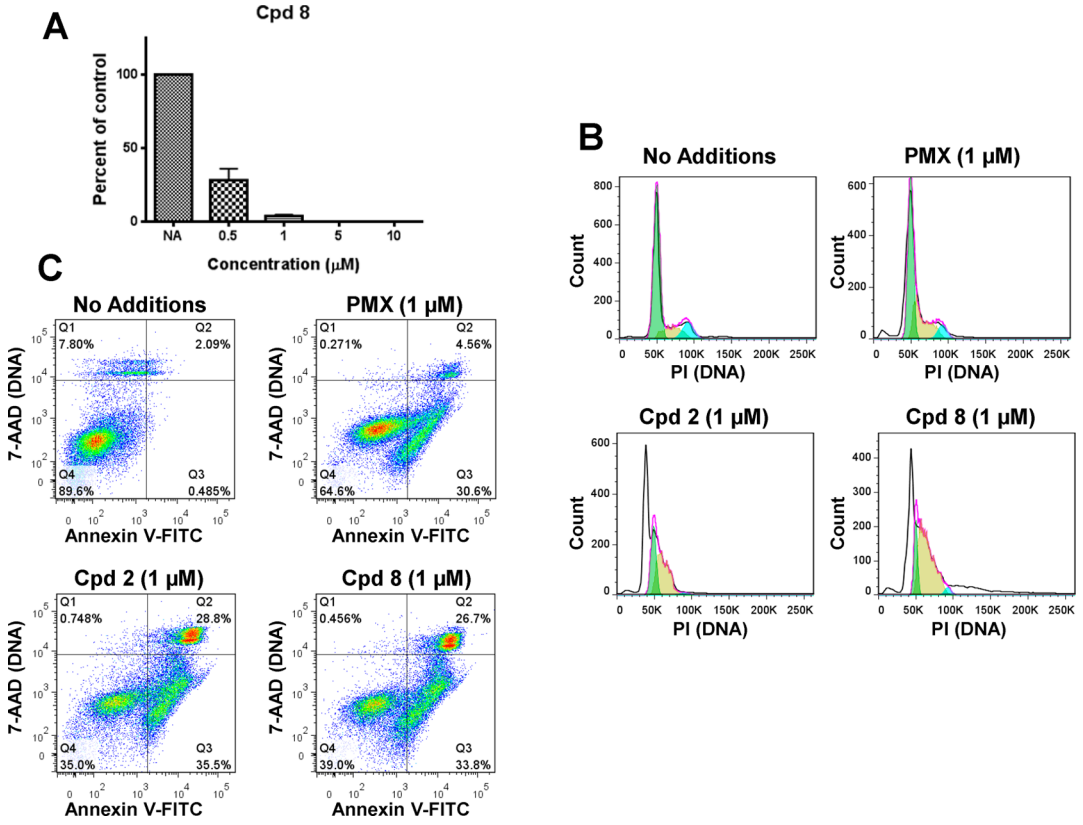

Figure 7. Inhibition of de novo purine biosynthesis by compound **8** results in cytotoxicity and apoptosis. (A) KB cells (1000 cells) were treated with compound **8** (0.5−10 μM) for 48 h, after which time the drug was removed and colonies were allowed to grow in drug-free medium over 10 days. Colonies were enumerated as described in the Experimental Section. The results are presented as mean values ± standard errors from three experiments. (B) Cell cycle analysis. KB cells were treated with 1 μM antifolate (PMX, compound **2**, or compound **8**) for 96 h, washed, fixed, and stained with PI. Cell cycle distributions were analyzed by flow cytometry. The sub-G_1 fraction (white fill) increased from 3.5% in the absence of drugs upon treatment with PMX (17.3%) or compounds **2** (45.1%) or **8** (36.7%). For the nonsub-G_1 population, the cell cycle distributions (colors are green for G_1/G_0, yellow for S, and blue for G_2/M) are as follows: no additions, 67.4% G_1/G_0, 15.9% S, 13.2% G_2/M; PMX, 47.8% G_1/G_0, 27.5% S, 7.5% G_2/M; compound **2**, 22.3% G_1/G_0, 31.4% S, 1.2% G_2/M; and compound **8**, 12.9% G_1/G_0, 48.2% S, 2.3% G_2/M. (C) Analysis of apoptosis by annexin V-FITC/7-AAD staining and flow cytometry is shown for KB cells treated with PMX or with compounds **2** or **8** for 96 h. The results are compared to those for controls treated with DMSO in lieu of drug. The percentages of cells in each quadrant (viable cells (annexin V-FITC^{low}/7-AAD^{low}; Q4), early apoptosis (annexin V-FITC^{high}/7-AAD^{low}; Q3), and late apoptosis/necrosis (annexin V-FITC^{high}/7-AAD^{high}; Q2)) are summarized.

for 48 h compared to levels of phospho-AMPK resulting from treatments with established AMPK activators including AICA, AICA ribonucleoside (AICAR), and metformin[24] (Figure 9B). Although KB cells are LKB1-null (the principal upstream kinase responsible for phosphorylating AMPK), AMPK is still activated upon treatment with known AMPK activators (Figure 9B). Although AMPK is activated by PMX, compound **8** was not significantly activating despite the accumulation of ZMP. Interestingly, neither AICA (not shown) nor metformin (Supporting Information, Figure 2S) at concentrations found to activate AMPK in Figure 9B (1 and 10 mM, respectively) were particularly growth inhibitory toward KB cells (20 and 32% inhibition, respectively).

Molecular Modeling: Docking Studies of Compound 8 with GARFTase and AICARFTase. On the basis of the cellular metabolic data that compound **8** inhibits both GARFTase and AICARFTase in KB cells (Figures 8 and 9, respectively), molecular modeling studies were performed. Molecular modeling of compound **8** used LeadIT 1.3.0 and was visualized using MOE 2011.10. Redocking the native crystal structure ligands 10-CF_3CO-DDACTHF[35] (Figure 10) for human GARFTase (PDB ID 1NJS) and BW2315, **18**,[36] (Figure 10) for AICARFTase (PDB ID 1PL0) into their respective crystal structures afforded docked poses with a rmsd ∼1 Å.

Figure 11 shows the docked pose of compound **8** in the human GARFTase active site. The cofactor binding pocket of GARFTase is located at the interface between the N-terminal mononucleotide binding domain and the C-terminal half of the structure. The binding site for the folate cofactor moiety consists of three parts: the pteridine binding cleft, the benzoylglutamate region, and the formyl transfer region. The docked pose shows the pyrrolo[2,3-*d*]pyrimidine scaffold of **8** to be buried deep in the active site and to occupy the same location as the diaminopyrimidone ring in the native crystal structure ligand (10-CF_3CO-DDACTHF). This orientation of the scaffold permits the 2-amino moiety to form hydrogen bonds to the backbone of Glu141 and Ser93. The N1 nitrogen interacts with the backbone of Leu92 to form a hydrogen bond. The 4-oxo moiety forms a hydrogen bond with Asp144 and forms water-mediated hydrogen bonds with Asp142 and Ala140 (not shown).

The molecule is oriented in a manner that aids the N7 nitrogen to form a hydrogen bond with Arg90. The pyrrolo[2,3-*d*]pyrimidine scaffold resides in a hydrophobic

dx.doi.org/10.1021/jm401328u | J. Med. Chem. 2013, 56, 10016−10032

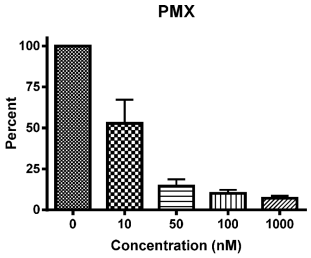

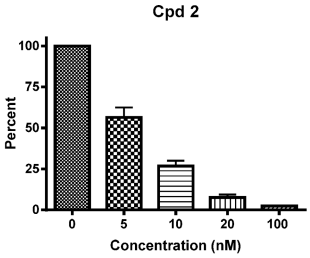

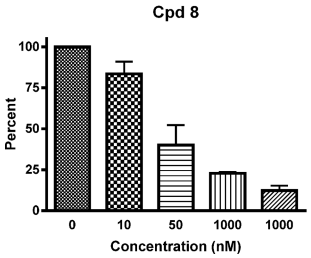

Antifolate	IC 50 (nM)
PMX	11.74 ± 6.64
Cpd 2	5.71 ± 1.19
Cpd 8	29.72 ± 10.59

Figure 8. In situ GARFTase assay. GARFTase activity and inhibition by 5- and 6-substituted pyrrolo[2,3-*d*]pyrimidine analogues **2**, **8**, and PMX were evaluated in situ with KB cells. Results are presented as mean values ± standard errors from three experiments. IC_{50}'s are summarized in the table. Additional details are described in the Experimental Section.

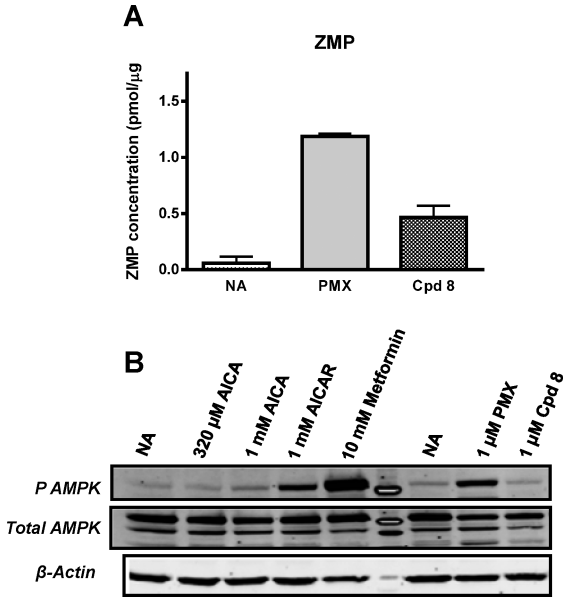

Figure 9. Accumulation of ZMP by 5-substituted pyrrolo[2,3-*d*]pyrimidines PMX and compound **8**. (A) ZMP (AICA ribonucleotide) accumulation was measured in KB cells treated for 48 h with the 5-substituted pyrrolo[2,3-*d*]pyrimidine antifolates **8** and PMX. Methods for extracting nucleotide metabolites and for measuring ZMP levels are detailed in the Experimental Section. The results are shown as mean values ± standard errors for three experiments. (B) KB cells were treated as indicated for 48 h followed by Western blot analysis of phosphorylated AMPK. Blots were probed with antibodies to phospho- and total AMPK as well as *β*-actin. Details are included in the Experimental Section. Abbreviations: AICA, 5-aminoimidazole-4-carboxamide; AICAR, 5-aminoimidazole-4-carboxamide ribonucleoside; and NA, no additions.

pocket formed by Leu85, Ile91 (not shown), Leu92, Val97, and the folate binding loop, residues 141–146. The flexible four-atom side chain helps to orient the benzoyl moiety of compound **8** into the benzoylglutamate region of the protein. The amide NH of the glutamate side chain forms a hydrogen bond with Met89. The *α*-carboxylic acid of the glutamate side chain interacts with Arg64 and additionally interacts with the backbone of Ile91. The *γ*-carboxylic acid can form a water-mediated hydrogen bond with Arg90. The interaction of the flexible glutamate side chain is very similar to the interaction network observed for the glutamate side chain of 10-CF_3CO-DDACTHF.

Figure 12 shows the overlay of the docked poses of **8** (blue) with the crystal structure ligand **18** (red) (a potent inhibitor) in human AICARFTase (PDB ID 1PL0). The pyrrolo[2,3-*d*]pyrimidine scaffold of **8** occupies the same location as the dihydroquinazoline scaffold of **18**. Analogous to **18**, the 2-NH_2 and N3 nitrogens of **8** interact with Asp546, whereas the 4-oxo moiety forms a hydrogen bond with the side chain of Asn547. The N7 nitrogen of **8** forms a hydrogen bond with the backbone of Met312. The pyrrolo[2,3-*d*]pyrimidine scaffold of **8** forms hydrophobic interactions with Met312, Phe315, Ile452, Pro543, and Phe544. The aryl glutamate section of **8** is oriented similarly to the phenyl glutamate side chain of **18**.

These docking results predict that **8** should bind and inhibit the two folate-dependent purine biosynthetic enzymes (GARFTase and AICARFTase) and are entirely consistent with the results of our in situ metabolic assays (Figures 8 and 9).

DISCUSSION

The development of rationally designed cytotoxic antifolates remains an area of significant interest to anticancer drug development, as exemplified by the relatively recent approval of PMX[37] and pralatrexate[38] for cancer therapy more than 50 years since the introduction of MTX.[1] Unfortunately, the ubiquitous presence of RFC may contribute to untoward toxicities of these classical antifolates toward normal tissues. On the basis of this, growing attention has focused on developing novel folate-based compounds with tumor targeting premised on transport selectivity for FRs or PCFT over RFC,[11,13−20] a pursuit that until recently[39,40] continued to be challenged by the lack of structural information on the major folate transport systems.

The antitumor efficacy for 5-substituted 2-carbon bridge pyrrolo[2,3-*d*]pyrimidine PMX reflects its cellular uptake by all of the major folate transport systems.[16−20] Although the corresponding 6-substituted analogue of PMX was pharmacologically inert, with increasing bridge lengths the 6-substituted pyrrolo[2,3-*d*]pyrimidines were surprisingly potent inhibitors of cell proliferation, but membrane transport by RFC was lost.[15,20] The 6-pyrrolo[2,3-*d*]pyrimidine benzoyl side-chain analogues with 3- and 4-bridge carbons (compounds **1** and **2**, respectively) were the most active of this series, reflecting their FR and PCFT cellular uptake with little to no transport by RFC as well as their potent inhibition of GARFTase, the first folate-dependent step in de novo purine nucleotide biosynthesis leading to the synthesis of IMP.[15,20] Inhibition of GARFTase resulted in decreased de novo synthesis of purine nucleotides and ATP depletion, leading to cytotoxicity and apoptosis.[15,20]

In this article, our goal was to establish further a comprehensive SAR for the 5- versus 6-substituted pyrrolo-[2,3-*d*]pyrimidine ring system in relation to folate transporter specificity and inhibition of intracellular targets based in part on findings of transporter promiscuity for PMX[16−20] and reports

dx.doi.org/10.1021/jm401328u | J. Med. Chem. 2013, 56, 10016−10032

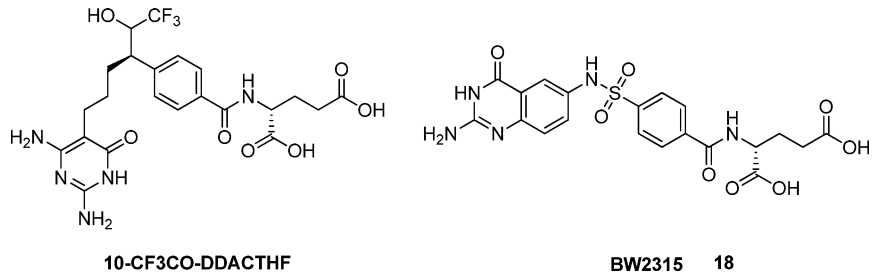

Figure 10. Structures of cocrystallized ligands 10-CF_3CO-DDACTHF (human GARFTase, PDB ID 1NJS) and BW2315 **18** (human AICARFTase, PDB ID 1PL0).

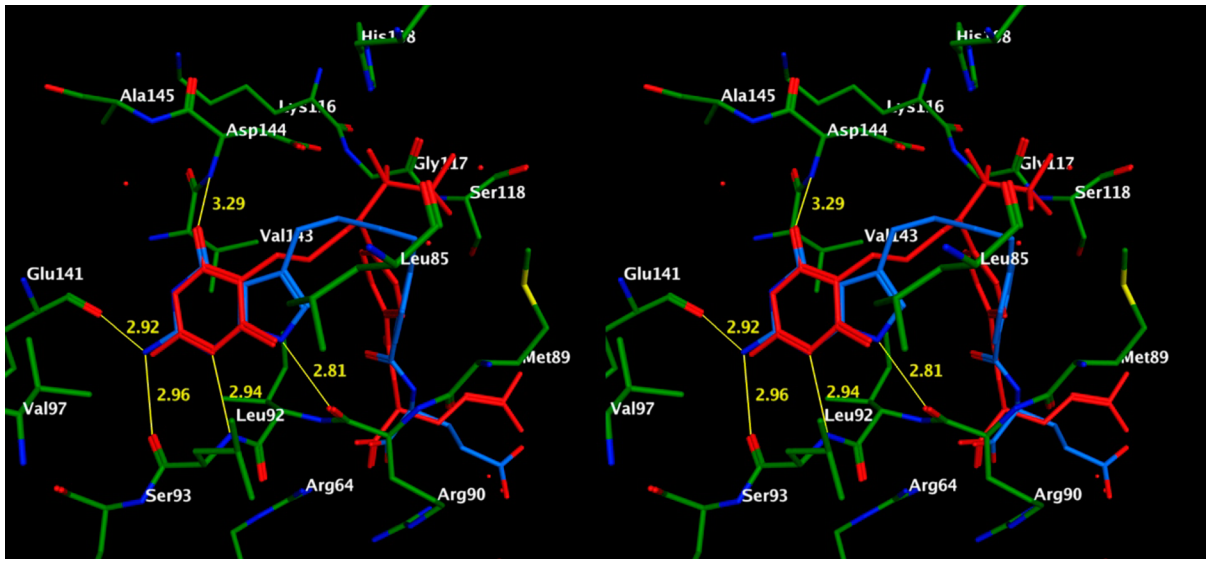

Figure 11. Stereoview overlay of the docked pose of compound **8** (blue) with 10-CF_3CO-DDACTHF (red) in human GARFTase (PDB ID 1NJS).

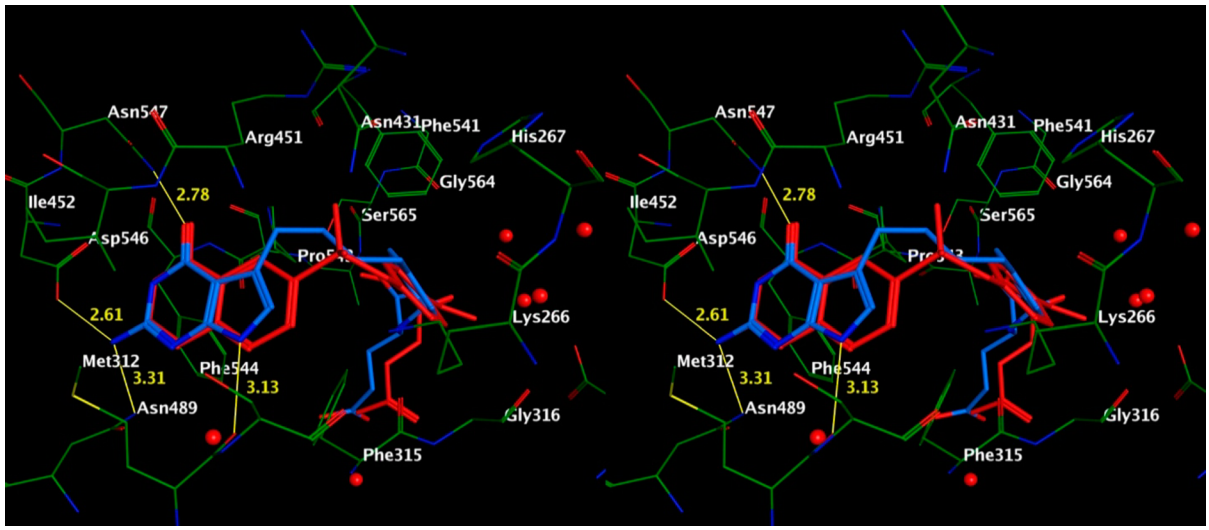

Figure 12. Stereoview overlay of the docked pose of compound **8** (blue) with **18** (red) in human AICARFTase (PDB ID 1PL0).

that PMX may in part derive its antitumor effects by inhibiting AICARTase, resulting in accumulation of ZMP and activation of AMPK in addition to inhibiting TS.[22,23] Compared to the 6-substituted analogues, we found that the 5-substituted pyrrolo-[2,3-*d*]pyrimidine compounds in general (i) were better substrates for RFC, with the highest antiproliferative activities for compounds with two-to-four bridge carbons independent of the nature of the side-chain ring system; (ii) were poorer substrates for PCFT with the exception of 2-carbon bridge compound PMX (**6**); and (iii) preserved FRα cellular uptake, with 4-carbon bridge analogue **8** showing the greatest FRα potency in this expanded 5-substituted series of analogues without TS inhibitory activity.

Compound **8** was cytotoxic, as reflected in the loss of clonogenicity in KB cells, and effected S-phase accumulation and apoptosis over 96 h. Like its 6-substituted counterpart

dx.doi.org/10.1021/jm401328u | *J. Med. Chem.* 2013, 56, 10016−10032

compound **1**,[20] compound **8** resulted in ATP depletion, although this appeared to be only partly due to inhibition of GARFTase. Rather, a unique feature of 5-substituted analogue **8** relates to its dual inhibition of both the GARFTase and AICARFTase reactions in de novo purine nucleotide biosynthesis. Although PMX also inhibited GARFTase, the finding that the AICARFTase substrate ZMP accumulates in the presence of this drug suggests that GARFTase inhibition must be incomplete and that AICARFTase must also be a target as previously described,[22,23] whereas for PMX, total purine nucleotides, as reflected in ATP pools, were significantly preserved. Compound **8** also inhibited AICARFTase, as reflected in the incomplete protection in cell proliferation assays by AICA, and demonstrated accumulation of the AICARFTase substrate ZMP, albeit to a lesser extent than for a comparable concentration of PMX. ATP pools were significantly depleted (~90%) with compound **8**.

Previous studies suggested that AMPK activation secondary to ZMP accumulation and AICARFTase inhibition may result in inhibition of mTOR and contribute to the antitumor effects of high levels of PMX in the presence of thymidine.[22,23] In the present study, we used KB tumor cells treated with PMX or with compound **8**. In this LKB1-deficient tumor cell line treated with PMX or compound **8**, ZMP accumulation was accompanied by AMPK activation in the presence of PMX but not compound **8**. AMPK activation was also seen upon treatment with AICA, AICAR, or metformin. However, ZMP accumulation and AMPK activation did not appear to be likely to contribute to the antiproliferative effects of PMX in KB cells, as neither AICA nor metformin (both of which activated AMPK more than PMX) potently inhibited cell proliferation. The antiproliferative and cytotoxic effects of compound **8** toward KB cells must derive from a depletion of ATP pools secondary to inhibition of both GARFTase and AICARFTase.

In summary, a series of classical 5-substituted pyrrolo[2,3-*d*]pyrimidine antifolates, **5**−**10**, was designed and synthesized as a hybrid of PMX and 6-substituted pyrrolo[2,3-*d*]-pyrimidines **1**−**4**. Compound **8**, the lead compound of this series, has an IC_{50} of 12.7 nM against KB tumor cells in culture. Rather than only targeting GARFTase, as with **1** and **2**, both GARFTase and AICARFTase were identified as the intracellular targets of **8**. Furthermore, on the basis of the patterns of inhibition of cell proliferation toward isogenic CHO cells expressing FRα or RFC, compound **8** appears to be transported by both FRα and RFC. The unique dual GARFTase and AICARFTase inhibition of compound **8** makes it an excellent lead compound for further study, including the design of additional antitumor analogues to optimize cellular folate uptake selectivity by FRs and inhibition of folate metabolizing enzymes, leading to a new generation of potent tumor-targeted agents. Furthermore, the dual enzyme inhibition results in potent inhibition of purine nucleotide biosynthesis and could preserve antitumor activity in the event that tumors become resistant as a result of alterations in one or the other targeted enzyme. Such dual-targeted inhibitors would seem to have substantial advantages over currently used agents that principally target only one intracellular enzyme target.

EXPERIMENTAL SECTION

All evaporations were carried out in vacuo with a rotary evaporator. Analytical samples were dried in vacuo (0.2 mmHg) in a CHEM-DRY drying apparatus over P_2O_5 at 80 °C. Melting points were determined on a MEL-TEMP II melting point apparatus with a FLUKE 51 K/J electronic thermometer and are uncorrected. Nuclear magnetic resonance spectra for proton (^{1}H NMR) were recorded on either a Bruker WH-400 (400 MHz) spectrometer or a Bruker WH-500 (500 MHz) spectrometer. The chemical-shift values are expressed in ppm (parts per million) relative to tetramethylsilane as an internal standard: s, singlet; d, doublet; t, triplet; q, quartet; m, multiplet; and br, broad singlet. Mass spectra were recorded on a VG-7070 double-focusing mass spectrometer or in a LKB-9000 instrument in the electron ionization (EI) mode. Chemical names follow IUPAC nomenclature. Thin-layer chromatography (TLC) was performed on Whatman Sil G/UV254 silica gel plates with a fluorescent indicator, and the spots were visualized under 254 and 365 nm illumination. All analytical samples were homogeneous on TLC in three different solvent systems. The proportions of solvents used for TLC are by volume. Column chromatography was performed on a 230−400 mesh silica gel (Fisher, Somerville, NJ) column. Elemental analyses were performed by Atlantic Microlab, Inc., Norcross, GA. Element compositions are within 0.4% of the calculated values. Fractional moles of water frequently found in the analytical sample of antifolates could not be prevented in spite of 24−48 h of drying in vacuo and were confirmed, where possible, by their presence in the ^{1}H NMR spectra. All solvents and chemicals were purchased from Aldrich Chemical Co. or Fisher Scientific and were used as received. For all of the compounds submitted for biological evaluation, elemental analysis (C,H, N) was performed to confirm >95% purity (Supporting Information, Table 1S).

Ethyl 4-(3-Oxopropyl)benzoate (13a). To a solution of ethyl 4-iodobenzoate (**11**) (5 mmol, 1.38 g) in 20 mL of anhydrous DMF were added prop-2-en-1-ol **12a** (6 mmol, 348 mg), LiCl (5 mmol, 210 mg), LiOAc (12.5 mmol, 850 mg), Bu_4NCl (2.5 mmol, 840 mg), and $Pd(OAc)_2$ (0.3 mmol, 60 mg), and the mixture was stirred at 70 °C for 3 h. TLC (hexane/EtOAc, 3:1) showed the disappearance of the starting material (R_f = 0.70) and formation of one major spot at R_f = 0.60. To the reaction mixture cooled to room temperature was added ethyl acetate (30 mL). The resulting solution was extracted with H_2O (10 mL × 3) and dried over Na_2SO_4. After evaporation of solvent, the residue was loaded on a silica gel column (4 × 20 cm) and flash-chromatographed with hexane/EtOAc (2:1), and the desired fractions were pooled. After evaporation of the solvent, the residue was dried in vacuo using P_2O_5 to afford **13a** (0.83 g, yield 83%) as a colorless liquid. R_f = 0.60 (hexane/EtOAc, 3:1). ^{1}H NMR (500 MHz, $CDCl_3$) δ 1.38 (t, 3H, CH_3, J = 7.0 Hz), 2.81 (t, 2H, CH_2, J = 7.5 Hz), 3.01 (t, 2H, CH_2, J = 7.5 Hz), 4.36 (q, 2H, CH_2, J = 7.0 Hz), 7.26 (d, 2H, 2 CH, J = 4.0 Hz), 7.97 (d, 2H, 2 CH, J = 4.3 Hz), 9.82 (t, 1H, CHO, J = 1.5 Hz).

Ethyl 4-(4-Oxobutyl)benzoate (13b). Compound **13b** was synthesized as described for **13a** (yield 88%) as a colorless liquid. R_f = 0.62 (hexane/EtOAc, 3:1). ^{1}H NMR (500 MHz, $CDCl_3$) δ 1.39 (t, 3H, CH_3, J = 7.0 Hz), 1.95−2.01 (m, 2H, CH_2), 2.46 (t, 2H, CH_2, J = 7.5 Hz), 2.71 (t, 2H, CH_2, J = 7.5 Hz), 4.37 (q, 2H, CH_2, J = 7.0 Hz), 7.24 (d, 2H, 2 CH, J = 4.3 Hz), 7.97 (d, 2H, 2 CH, J = 4.3 Hz), 9.76 (t, 1H, CHO, J = 1.5 Hz).

Ethyl 4-(5-Oxopentyl)benzoate (13c). Compound **13c** was synthesized as described for **13a**: (yield 84%) as a colorless liquid. R_f = 0.62 (hexane/EtOAc, 3:1). ^{1}H NMR (500 MHz, $CDCl_3$) δ 1.38 (t, 3H, CH_3, J = 7.0 Hz), 1.66−1.70 (m, 4H, 2 CH_2), 2.46 (t, 2H, CH_2, J = 7.0 Hz), 2.69 (t, 2H, CH_2, J = 7.0 Hz), 4.36 (q, 2H, CH_2, J = 7.0 Hz), 7.23 (d, 2H, 2 CH, J = 4.0 Hz), 7.96 (d, 2H, 2 CH, J = 4.0 Hz), 9.75 (t, 1H, CHO, J = 1.5 Hz).

Ethyl 4-(6-Oxohexyl)benzoate (13d). Compound **13d** was synthesized as described for **13a** (yield 86%) as a colorless liquid. R_f = 0.62 (hexane/EtOAc, 3:1). ^{1}H NMR (500 MHz, $CDCl_3$) δ 1.25−1.27 (m, 2H, CH_2), 1.38 (t, 3H, CH_3, J = 7.0 Hz), 1.64−1.68 (m, 4H, 2 CH_2), 2.42 (t, 2H, CH_2, J = 7.5 Hz), 2.66 (t, 2H, CH_2, J = 7.5 Hz), 4.36 (q, 2H, CH_2, J = 7.0 Hz), 7.23 (d, 2H, 2 CH, J = 4.3 Hz), 7.96 (d, 2H, 2 CH, J = 4.3 Hz), 9.75 (t, 1H, CHO, J = 2.0 Hz).

Ethyl 4-(7-Oxoheptyl)benzoate (13e). Compound **13e** was synthesized as described for **13a** (yield 92%) as a colorless liquid. R_f = 0.63 (hexane/EtOAc, 3:1). ^{1}H NMR (500 MHz, $CDCl_3$) δ 1.34−1.36 (m, 4H, 2 CH_2), 1.38 (t, 3H, CH_3, J = 7.0 Hz), 1.58−1.65 (m, 4H, 2

CH_2), 2.42 (t, 2H, CH_2, J = 7.5 Hz), 2.66 (t, 2H, CH_2, J = 7.5 Hz), 4.36 (q, 2H, CH_2, J = 7.0 Hz), 7.23 (d, 2H, 2 CH, J = 4.3 Hz), 7.95 (d, 2H, 2 CH, J = 4.3 Hz), 9.75 (t, 1H, CHO, J = 2.0 Hz).

Ethyl 4-(8-Oxooctyl)benzoate (13f). Compound **13f** was synthesized as described for **13a** (yield 87%) as a colorless liquid. R_f = 0.63 (hexane/EtOAc, 3:1). ^{1}H NMR (500 MHz, $CDCl_3$) δ 1.28−1.34 (m, 6H, 3 CH_2), 1.38 (t, 3H, CH_3, J = 7.0 Hz), 1.60−1.63 (m, 4H, 2 CH_2), 2.42 (t, 2H, CH_2, J = 7.5 Hz), 2.64 (t, 2H, CH_2, J = 7.5 Hz), 4.36 (q, 2H, CH_2, J = 7.0 Hz), 7.23 (d, 2H, 2 CH, J = 4.3 Hz), 7.95 (d, 2H, 2 CH, J = 4.3 Hz), 9.75 (t, 1H, CHO, J = 2.0 Hz).

Ethyl 4-(3-Bromo-4-oxobutyl)benzoate (14b). To a solution of aldehyde **13b** (1 mmol, 220 mg) in 5 mL of anhydrous Et_2O were added 5,5-dibromo-2,2-dimethyl-4,6-dioxo-1,3-dioxane (0.5 mmol, 150 mg) and 2 N HCl in Et_2O solution (0.1 mmol, 50 μL), and the mixture was stirred at room temperature for 24 h. TLC (hexane/EtOAc, 3:1) showed the disappearance of the starting material (R_f = 0.62) and formation of one major spot at R_f = 0.50. The reaction solution was washed with 5% $NaHCO_3$ solution, extracted with H_2O (10 mL × 3), and dried over Na_2SO_4. After evaporation of the solvent, the residue was loaded on a silica gel column (4 × 20 cm) and flash-chromatographed with hexane/EtOAc (2:1), and the desired fractions were pooled. After evaporation of the solvent, the residue was dried in vacuo using P_2O_5 to afford **14b** (235 mg, yield 78%) as a colorless oil. R_f = 0.50 (hexane/EtOAc, 3:1). ^{1}H NMR (500 MHz, $CDCl_3$) δ 1.39 (t, 3H, CH_3, J = 7.0 Hz), 2.19−2.27 (m, 1H, CH_2), 2.34−2.42 (m, 1H, CH_2), 2.79−2.85 (m, 1H, CH_2), 2.91−2.97 (m, 1H, CH_2), 4.16−4.18 (m, 1H, CHBr), 4.37 (q, 2H, CH_2, J = 7.0 Hz), 7.28 (d, 2H, 2 CH, J = 4.3 Hz), 7.99 (d, 2H, 2 CH, J = 4.3 Hz), 9.46 (d, 1H, CHO, J = 1.0 Hz).

Ethyl 4-(2-Bromo-3-oxopropyl)benzoate (14a). Compound **14a** was synthesized as described for **14b. 14a** is not stable and was used directly in the next step without purification.

Ethyl 4-(4-Bromo-5-oxopentyl)benzoate (14c). Compound **14c** was synthesized as described for **14b** (yield 77%) as a colorless oil. R_f = 0.52 (hexane/EtOAc, 3:1). ^{1}H NMR (500 MHz, $CDCl_3$) δ 1.39 (t, 3H, CH_3, J = 7.0 Hz), 1.73−1.82 (m, 2H, CH_2), 1.86−1.96 (m, 1H, CH_2), 2.03−2.10 (m, 1H, CH_2), 2.71−2.75 (m, 2H, CH_2), 4.21−4.25 (m, 1H, CHBr), 4.37 (q, 2H, CH_2, J = 7.0 Hz), 7.24 (d, 2H, 2 CH, J = 4.3 Hz), 7.97 (d, 2H, 2 CH, J = 4.3 Hz), 9.42 (d, 1H, CHO, J = 1.3 Hz).

Ethyl 4-(5-Bromo-6-oxohexyl)benzoate (14d). Compound **14d** was synthesized as described for **14b** (yield 75%) as a colorless oil. R_f = 0.52 (hexane/EtOAc, 3:1). ^{1}H NMR (400M, $CDCl_3$) δ 1.39 (t, 3H, CH_3, J = 7.0 Hz), 1.63−1.75 (m, 4H, 2 CH_2), 1.87−1.99 (m, 1H, CH_2), 2.03−2.12 (m, 1H, CH_2), 2.69 (t, 2H, CH_2, J = 7.0 Hz), 4.19−4.22 (m, 1H, CHBr), 4.36 (q, 2H, CH_2, J = 7.0 Hz), 7.23 (d, 2H, 2 CH, J = 4.0 Hz), 7.96 (d, 2H, 2 CH, J = 4.0 Hz), 9.42 (d, 1H, CHO, J = 1.2 Hz).

Ethyl 4-(6-Bromo-7-oxoheptyl)benzoate (14e). Compound **14e** was synthesized as described for **14b** (yield 77%) as a colorless oil. R_f = 0.54 (hexane/EtOAc, 3:1). ^{1}H NMR (500 MHz, $CDCl_3$) δ 1.30−1.40 (m, 2H, CH_2), 1.38 (t, 3H, CH_3, J = 7.0 Hz), 1.62−1.70 (m, 4H, 2 CH_2), 1.86−1.94 (m, 1H, CH_2), 2.00−2.07 (m, 1H, CH_2), 2.66 (t, 2H, CH_2, J = 7.5 Hz), 4.18−4.22 (m, 1H, CHBr), 4.36 (q, 2H, CH_2, J = 7.0 Hz), 7.23 (d, 2H, 2 CH, J = 4.3 Hz), 7.95 (d, 2H, 2 CH, J = 4.0 Hz), 9.42 (d, 1H, CHO, J = 1.5 Hz).

Ethyl 4-(7-Bromo-8-oxooctyl)benzoate (14f). Compound **14f** was synthesized as described for **14b** (yield 74%) as a colorless oil. R_f = 0.56 (hexane/EtOAc, 3:1). ^{1}H NMR (500 MHz, $CDCl_3$) δ 1.30−1.40 (m, 4H, 2 CH_2), 1.38 (t, 3H, CH_3, J = 7.0 Hz), 1.62−1.64 (m, 4H, 2 CH_2), 1.86−1.94 (m, 1H, CH_2), 2.00−2.07 (m, 1H, CH_2), 2.65 (t, 2H, CH_2, J = 7.5 Hz), 4.19−4.22 (m, 1H, CHBr), 4.36 (q, 2H, CH_2, J = 7.0 Hz), 7.23 (d, 2H, 2 CH, J = 4.0 Hz), 7.95 (d, 2H, 2 CH, J = 4.0 Hz), 9.42 (d, 1H, CHO, J = 1.5 Hz).

Ethyl 4-(2-(2-Amino-4-oxo-4,7-dihydro-3*H*-pyrrolo[2,3-*d*]-pyrimidin-5-yl)ethyl)benzoate (16b). To a solution of 2,6-diamino-64-oxopyrimidine **15** (151 mg, 1.2 mmol) and sodium acetate (180 mg, 2.2 mmol) in water (3 mL) and methanol (3 mL) was added α-bromo aldehyde **14b** (330 mg, 1.1 mmol) The reaction mixture was stirred at 45 °C for 3 h. TLC showed the disappearance of starting materials and the formation of one major spot at R_f = 0.38 ($CHCl_3$/MeOH, 5:1). After evaporation of the solvent, CH_3OH (10 mL) was added followed by silica gel (3 g). Evaporation of the solvent afforded a plug, which was loaded onto a silica gel column (3.5 cm × 15 cm) and eluted initially with $CHCl_3$ followed by 10% MeOH in $CHCl_3$ and then 15% MeOH in $CHCl_3$. Fractions showing R_f = 0.38 were pooled and evaporated to afford **16b** (230 mg, yield 70%) as a pink solid. mp > 250 °C decomposed. ^{1}H NMR (500 MHz, DMSO-d_6) δ 1.30 (t, 3H, CH_3, J = 7.5 Hz), 2.84 (t, 2H, CH_2, J = 7.0 Hz), 2.99 (t, 2H, CH_2, J = 7.0 Hz), 4.29 (q, 2H, CH_2, J = 7.5 Hz), 6.03 (s, 2H, 2-NH_2), 6.29 (d, 1H, CH, J = 1.0 Hz), 7.33 (d, 2H, CH, J = 4.0 Hz), 7.85 (d, 2H, CH, J = 4.0 Hz), 10.21 (s, 1H, 3-NH), 10.60 (s, 1H, 7-NH).

Ethyl 4-((2-Amino-4-oxo-4,7-dihydro-3*H*-pyrrolo[2,3-*d*]-pyrimidin-5-yl)methyl)benzoate (16a). Compound **16a** was synthesized as described for **16b** (yield 35%) over two steps as a yellow solid. mp > 232 °C decomposed. R_f = 0.42 ($CHCl_3$/MeOH, 5:1). ^{1}H NMR (500 MHz, DMSO-d_6) δ 1.29 (t, 3H, CH_3, J = 7.5 Hz), 4.00 (s, 2H, CH_2), 4.28 (q, 2H, CH_2, J = 7.5 Hz), 6.00 (s, 2H, 2-NH_2), 6.34 (d, 1H, CH, J = 1.0 Hz), 7.41 (d, 2H, CH, J = 4.0 Hz), 7.83 (d, 2H, CH, J = 4.0 Hz), 10.12 (s, 1H, 3-NH), 10.74 (s, 1H, 7-NH).

Ethyl 4-(3-(2-Amino-4-oxo-4,7-dihydro-3*H*-pyrrolo[2,3-*d*]-pyrimidin-5-yl)propyl)benzoate (16c). Compound **16c** was synthesized as described for **16b** (yield 68%) as a purple solid. mp > 264 °C decomposed. R_f = 0.42 ($CHCl_3$/MeOH, 5:1). ^{1}H NMR (500 MHz, DMSO-d_6) δ 1.30 (t, 3H, CH_3, J = 7.5 Hz), 1.89−1.95 (m, 2H, CH_2), 2.57 (t, 2H, CH_2, J = 7.5 Hz), 2.66 (t, 2H, CH_2, J = 7.5 Hz), 4.29 (q, 2H, CH_2, J = 7.5 Hz), 5.96 (s, 2H, 2-NH_2), 6.35 (d, 1H, CH, J = 1.0 Hz), 7.34 (d, 2H, CH, J = 4.0 Hz), 7.86 (d, 2H, CH, J = 4.0 Hz), 10.08 (s, 1H, 3-NH), 10.63 (s, 1H, 7-NH).

Ethyl 4-(4-(2-Amino-4-oxo-4,7-dihydro-3*H*-pyrrolo[2,3-*d*]-pyrimidin-5-yl)butyl)benzoate (16d). Compound **16d** was synthesized as described for **16b** (yield 53%) as a blue solid. mp > 256 °C decomposed. R_f = 0.44 ($CHCl_3$/MeOH, 5:1). ^{1}H NMR (500 MHz, DMSO-d_6) δ 1.30 (t, 3H, CH_3, J = 7.5 Hz), 1.56−1.62 (m, 4H, 2 CH_2), 2.58 (t, 2H, CH_2, J = 7.5 Hz), 2.65 (t, 2H, CH_2, J = 7.5 Hz), 4.29 (q, 2H, CH_2, J = 7.5 Hz), 5.94 (s, 2H, 2-NH_2), 6.31 (d, 1H, CH, J = 1.0 Hz), 7.33 (d, 2H, CH, J = 4.0 Hz), 7.85 (d, 2H, CH, J = 4.0 Hz), 10.08 (s, 1H, 3-NH), 10.59 (s, 1H, 7-NH).

Ethyl 4-(5-(2-Amino-4-oxo-4,7-dihydro-3*H*-pyrrolo[2,3-*d*]-pyrimidin-5-yl)pentyl)benzoate (16e). Compound **16e** was synthesized as described for **16b** (yield 60%) as a pink solid. mp > 212 °C decomposed. R_f = 0.45 ($CHCl_3$/MeOH, 5:1). ^{1}H NMR (500 MHz, DMSO-d_6) δ 1.29−1.32 (m, 5H, CH_3, CH_2), 1.58−1.62 (m, 4H, 2 CH_2), 2.53 (t, 2H, CH_2, J = 7.5 Hz), 2.63 (t, 2H, CH_2, J = 7.5 Hz), 4.29 (q, 2H, CH_2, J = 7.5 Hz), 5.94 (s, 2H, 2-NH_2), 6.30 (d, 1H, CH, J = 1.0 Hz), 7.33 (d, 2H, CH, J = 4.0 Hz), 7.85 (d, 2H, CH, J = 4.0 Hz), 10.08 (s, 1H, 3-NH), 10.58 (s, 1H, 7-NH).

Ethyl 4-(6-(2-Amino-4-oxo-4,7-dihydro-3*H*-pyrrolo[2,3-*d*]-pyrimidin-5-yl)hexyl)benzoate (16f). Compound **16f** was synthesized as described for **16b** (yield 52%) as a pink solid. mp > 208 °C decomposed. R_f = 0.45 ($CHCl_3$/MeOH, 5:1). ^{1}H NMR (500 MHz, DMSO-d_6) δ 1.27−1.33 (m, 7H, CH_3, 2 CH_2), 1.53−1.60 (m, 4H, 2 CH_2), 2.53 (t, 2H, CH_2, J = 7.5 Hz), 2.62 (t, 2H, CH_2, J = 7.5 Hz), 4.29 (q, 2H, CH_2, J = 7.5 Hz), 5.94 (s, 2H, 2-NH_2), 6.30 (d, 1H, CH, J = 1.0 Hz), 7.33 (d, 2H, CH, J = 4.0 Hz), 7.86 (d, 2H, CH, J = 4.0 Hz), 10.06 (s, 1H, 3-NH), 10.57 (s, 1H, 7-NH).

(*S*)-Diethyl 2-(4-((2-Amino-4-oxo-4,7-dihydro-3*H*-pyrrolo-[2,3-*d*]pyrimidin-5-yl)methyl)benzamido)pentanedioate (17a). To a suspension of **16a** (100 mg, 0.35 mmol) in 10 mL of CH_3OH was added 3 N NaOH (10 mL). The resulting mixture was stirred under N_2 at 40−50 °C for 24 h. TLC indicated the disappearance of starting material and the formation of one major spot at the origin. The resulting solution was passed through Celite and washed with a minimum amount of CH_3OH. The combined filtrate was evaporated under reduced pressure to dryness. To this residue was added distilled water (10 mL). The solution was cooled in an ice bath, and the pH was adjusted 3 to 4 using 3 N HCl. The resulting suspension was chilled in a dry ice/acetone bath and thawed to 4 °C overnight in a refrigerator. The precipitate was filtered, washed with cold water, and

dx.doi.org/10.1021/jm401328u | J. Med. Chem. 2013, 56, 10016−10032

dried in a desiccator under reduced pressure using P_2O_5 to a brown powder, which was used directly for the next step. To a solution of this brown powder in anhydrous DMF (10 mL) were added 6-chloro-2,4-dimethoxy-1,3,5-triazine (72 mg, 0.42 mmol) and *N*-methylmorpholine (43 mg, 0.42 mmol). After the mixture was stirred at rt for 2 h, *N*-methylmorpholine (43 mg, 0.42 mmol) and dimethyl L-glutamate hydrochloride (126 mg, 0.53 mmol) were added all at once. The mixture was stirred at rt for 4 h. TLC showed the formation of one major spot at R_f = 0.38 ($CHCl_3$/MeOH, 5:1). The reaction mixture was evaporated to dryness under reduced pressure. The residue was dissolved in a minimum amount of $CHCl_3$/MeOH, 5:1, and chromatographed on a silica gel column (2 cm × 15 cm) with 4% MeOH in $CHCl_3$ as the eluent. Fractions that showed the desired single spot at R_f = 0.38 were pooled and evaporated to dryness to afford **17a** (100 mg, yield 61%) as a yellow syrup. ^{1}H NMR (400M, DMSO-d_6) δ 1.14−1.19 (m, 6H, 2 CH_3), 1.88−2.15 (m, 2H, CH_2), 2.42−2.45 (m, 2H, CH_2), 3.98 (s, 2H, CH_2), 4.03−4.12 (m, 4H, 2 CH_2), 4.36−4.46 (m, 1H, CH), 6.00 (s, 2H, 2-NH_2), 6.32 (d, 1H, CH, J = 1.0 Hz), 7.37 (d, 2H, C_6H_4, J = 4.0 Hz), 7.74 (d, 2H, C_6H_4, J = 4.0 Hz), 8.60 (d, 1H, CONH, J = 4.0 Hz), 10.13 (s, 1H, 3-NH), 10.74 (s, 1H, 7-NH).

(*S*)-Diethyl 2-(4-(2-(2-Amino-4-oxo-4,7-dihydro-3*H*-pyrrolo-[2,3-*d*]pyrimidin-5-yl)ethyl)benzamido)pentanedioate (17b). Compound **17b** was synthesized as described for **17a** (yield 51%) as a colorless syrup. R_f = 0.40 ($CHCl_3$/MeOH, 5:1). ^{1}H NMR (500 MHz, DMSO-d_6) δ 1.15−1.20 (m, 6H, 2 CH_3), 1.97−2.03 (m, 1H, CH_2), 2.06−2.13 (m, 1H, CH_2), 2.42−2.45 (m, 2H, CH_2), 2.85 (t, 2H, CH_2, J = 7.0 Hz), 2.97 (t, 2H, CH_2, J = 7.0 Hz), 4.02−4.13 (m, 4H, 2 CH_2), 4.40−4.44 (m, 1H, CH), 5.99 (s, 2H, 2-NH_2), 6.30 (d, 1H, CH, J = 1.0 Hz), 7.29 (d, 2H, C_6H_4, J = 4.0 Hz), 7.77 (d, 2H, C_6H_4, J = 4.0 Hz), 8.61 (d, 1H, CONH, J = 4.0 Hz), 10.13 (s, 1H, 3-NH), 10.60 (s, 1H, 7-NH).

(*S*)-Diethyl 2-(4-(3-(2-Amino-4-oxo-4,7-dihydro-3*H*-pyrrolo-[2,3-*d*]pyrimidin-5-yl)propyl)benzamido)pentanedioate (17c). Compound **17c** was synthesized as described for **17a** (yield 65%) as a colorless syrup. R_f = 0.40 ($CHCl_3$/MeOH, 5:1). ^{1}H NMR (DMSO-d_6) δ 1.15−1.20 (m, 6H, 2 CH_3), 1.91−1.94 (m, 2H, CH_2), 1.97−2.03 (m, 1H, CH_2), 2.06−2.13 (m, 1H, CH_2), 2.42−2.45 (m, 2H, CH_2), 2.58 (t, 2H, CH_2, J = 7.0 Hz), 2.64 (t, 2H, CH_2, J = 7.0 Hz), 4.02−4.13 (m, 4H, 2 CH_2), 4.42−4.45 (m, 1H, CH), 5.95 (s, 2H, 2-NH_2), 6.35 (d, 1H, CH, J = 1.0 Hz), 7.29 (d, 2H, C_6H_4, J = 4.0 Hz), 7.79 (d, 2H, C_6H_4, J = 4.0 Hz), 8.63 (d, 1H, CONH, J = 4.0 Hz), 10.08 (s, 1H, 3-NH), 10.62 (s, 1H, 7-NH).

(*S*)-Diethyl 2-(4-(4-(2-Amino-4-oxo-4,7-dihydro-3*H*-pyrrolo-[2,3-*d*]pyrimidin-5-yl)butyl)benzamido)pentanedioate (17d). Compound **17d** was synthesized as described for **17a** (yield 70%) as a light blue syrup. R_f = 0.40 ($CHCl_3$/MeOH, 5:1). ^{1}H NMR (500 MHz, DMSO-d_6) δ 1.15−1.20 (m, 6H, 2 CH_3), 1.55−1.64 (m, 4H, 2 CH_2), 1.97−2.03 (m, 1H, CH_2), 2.06−2.13 (m, 1H, CH_2), 2.42−2.45 (m, 2H, CH_2), 2.58 (t, 2H, CH_2, J = 7.5 Hz), 2.65 (t, 2H, CH_2, J = 7.5 Hz), 4.02−4.13 (m, 4H, 2 CH_2), 4.42−4.45 (m, 1H, CH), 5.94 (s, 2H, 2-NH_2), 6.31 (d, 1H, CH, J = 1.0 Hz), 7.28 (d, 2H, C_6H_4, J = 4.0 Hz), 7.77 (d, 2H, C_6H_4, J = 4.0 Hz), 8.61 (d, 1H, CONH, J = 4.0 Hz), 10.08 (s, 1H, 3-NH), 10.59 (s, 1H, 7-NH).

(*S*)-Diethyl 2-(4-(5-(2-Amino-4-oxo-4,7-dihydro-3*H*-pyrrolo-[2,3-*d*]pyrimidin-5-yl)pentyl)benzamido)pentanedioate (17e). Compound **17e** was synthesized as described for **17a** (yield 67%) as a light blue syrup. R_f = 0.40 ($CHCl_3$/MeOH, 5:1). ^{1}H NMR (500 MHz, DMSO-d_6) δ 1.15−1.20 (m, 6H, 2 CH_3), 1.29−1.33 (m, 2H, CH_2), 1.55−1.62 (m, 4H, 2 CH_2), 1.97−2.03 (m, 1H, CH_2), 2.06−2.13 (m, 1H, CH_2), 2.42−2.45 (m, 2H, CH_2), 2.51−2.53 (m, 2H, CH_2), 2.62 (t, 2H, CH_2, J = 7.5 Hz), 4.02−4.12 (m, 4H, 2 CH_2), 4.41−4.45 (m, 1H, CH), 5.94 (s, 2H, 2-NH_2), 6.31 (d, 1H, CH, J = 1.0 Hz), 7.28 (d, 2H, C_6H_4, J = 4.0 Hz), 7.78 (d, 2H, C_6H_4, J = 4.0 Hz), 8.62 (d, 1H, CONH, J = 4.0 Hz), 10.07 (s, 1H, 3-NH), 10.58 (s, 1H, 7-NH).

(*S*)-Diethyl 2-(4-(6-(2-Amino-4-oxo-4,7-dihydro-3*H*-pyrrolo-[2,3-*d*]pyrimidin-5-yl)hexyl)benzamido)pentanedioate (17f). Compound **17f** was synthesized as described for **17a** (yield 78%) as a colorless syrup. R_f = 0.42 ($CHCl_3$/MeOH, 5:1). ^{1}H NMR (500 MHz, DMSO-d_6) δ 1.15−1.20 (m, 6H, 2 CH_3), 1.27−1.34 (m, 4H, 2 CH_2), 1.53−1.62 (m, 4H, 2 CH_2), 1.97−2.03 (m, 1H, CH_2), 2.06−2.13 (m, 1H, CH_2), 2.42−2.45 (m, 2H, CH_2), 2.51−2.53 (m, 2H, CH_2), 2.61 (t, 2H, CH_2, J = 7.5 Hz), 4.02−4.12 (m, 4H, 2 CH_2), 4.41−4.44 (m, 1H, CH), 5.93 (s, 2H, 2-NH_2), 6.30 (d, 1H, CH, J = 1.0 Hz), 7.28 (d, 2H, C_6H_4, J = 4.0 Hz), 7.78 (d, 2H, C_6H_4, J = 4.0 Hz), 8.62 (d, 1H, CONH, J = 4.0 Hz), 10.06 (s, 1H, 3-NH), 10.57 (s, 1H, 7-NH).

(*S*)-2-(4-((2-Amino-4-oxo-4,7-dihydro-3*H*-pyrrolo[2,3-*d*]-pyrimidin-5-yl)methyl)benzamido)pentanedioic Acid (5). To **17a** (75 mg, 0.26 mmol) was added 1 N NaOH (3 mL). The resulting mixture was stirred at rt for 2 h. TLC indicated the disappearance of starting material and the formation of one major spot at the origin. The resulting solution was passed through Celite. The combined filtrate was evaporated under reduced pressure to dryness. To this residue was added distilled water (10 mL). The solution was cooled in an ice bath, and the pH was adjusted 3 to 4 using 1 N HCl. The resulting suspension was chilled in a dry ice/acetone bath and thawed to 4 °C overnight in a refrigerator. The precipitate was filtered, washed with cold water, and dried in a desiccator under reduced pressure using P_2O_5 (yield 94%) as a yellow powder. mp > 264 °C decomposed. R_f = 0.05 ($CHCl_3$/MeOH, 5:1). ^{1}H NMR (400 MHz, DMSO-d_6) δ 1.88−2.15 (m, 2H, CH_2), 2.42−2.45 (m, 2H, CH_2), 3.98 (s, 2H, CH_2), 4.37−4.39 (m, 1H, CH), 6.00 (s, 2H, 2-NH_2), 6.32 (s, 1H, CH), 7.37 (d, 2H, C_6H_4, J = 4.0 Hz), 7.75 (d, 2H, C_6H_4, J = 4.0 Hz), 8.47 (d, 1H, CONH, J = 4.0 Hz), 10.13 (s, 1H, 3-NH), 10.73 (s, 1H, 7-NH). Anal. ($C_{19}H_{19}N_5O_6\cdot 1.5H_2O$).

(*S*)-2-(4-(2-(2-Amino-4-oxo-4,7-dihydro-3*H*-pyrrolo[2,3-*d*]-pyrimidin-5-yl)ethyl)benzamido)pentanedioic Acid (6). Compound **6** was synthesized as described for **5** (yield 96%) as a pink powder. mp > 250 °C decomposed. Identical in all respects (NMR, mp) to that reported by the method of Taylor et al.[41] R_f = 0.07 ($CHCl_3$/MeOH, 5:1). ^{1}H NMR (400 MHz , DMSO-d_6) δ 1.97−2.03 (m, 1H, CH_2), 2.06−2.13 (m, 1H, CH_2), 2.42−2.45 (m, 2H, CH_2), 2.85 (t, 2H, CH_2, J = 7.0 Hz), 2.97 (t, 2H, CH_2, J = 7.0 Hz), 4.36−4.40 (m, 1H, CH), 6.00 (s, 2H, 2-NH_2), 6.30 (s, 1H, CH), 7.28 (d, 2H, C_6H_4, J = 4.0 Hz), 7.78 (d, 2H, C_6H_4, J = 4.0 Hz), 8.51 (d, 1H, CONH, J = 4.0 Hz), 10.15 (s, 1H, 3-NH), 10.61 (s, 1H, 7-NH). Anal. ($C_{20}H_{21}N_5O_6\cdot 1.2H_2O$).

(*S*)-2-(4-(3-(2-Amino-4-oxo-4,7-dihydro-3*H*-pyrrolo[2,3-*d*]-pyrimidin-5-yl)propyl)benzamido)pentanedioic Acid (7). Compound **7** was synthesized as described for **5** (yield 97%) as a pale-blue powder. mp > 189 °C decomposed. R_f = 0.07 ($CHCl_3$/MeOH, 5:1). ^{1}H NMR (500 MHz, DMSO-d_6) δ 1.90−1.94 (m, 2H, CH_2), 1.94−2.00 (m, 1H, CH_2), 2.06−2.13 (m, 1H, CH_2), 2.33−2.36 (m, 2H, CH_2), 2.58 (t, 2H, CH_2, J = 7.0 Hz), 2.64 (t, 2H, CH_2, J = 7.0 Hz), 4.36−4.40 (m, 1H, CH), 5.96 (s, 2H, 2-NH_2), 6.35 (d, 1H, CH, J = 1.0 Hz), 7.29 (d, 2H, C_6H_4, J = 4.0 Hz), 7.79 (d, 2H, C_6H_4, J = 4.0 Hz), 8.51 (d, 1H, CONH, J = 4.0 Hz), 10.08 (s, 1H, 3-NH), 10.62 (s, 1H, 7-NH). Anal. ($C_{21}H_{23}N_5O_6\cdot 0.70H_2O$).

(*S*)-2-(4-(4-(2-Amino-4-oxo-4,7-dihydro-3*H*-pyrrolo[2,3-*d*]-pyrimidin-5-yl)butyl)benzamido)pentanedioic Acid (8). Compound **8** was synthesized as described for **5** (yield 88%) as a blue powder. mp > 153 °C decomposed. R_f = 0.07 ($CHCl_3$/MeOH, 5:1). ^{1}H NMR (500 MHz, DMSO-d_6) δ 1.55−1.63 (m, 4H, 2 CH_2), 1.92−2.00 (m, 1H, CH_2), 2.03−2.13 (m, 1H, CH_2), 2.34 (t, 2H, CH_2, J = 7.5 Hz), 2.58 (t, 2H, CH_2, J = 7.5 Hz), 2.63 (t, 2H, CH_2, J = 7.5 Hz), 4.37−4.39 (m, 1H, CH), 5.95 (s, 2H, 2-NH_2), 6.31 (d, 1H, CH, J = 1.0 Hz), 7.28 (d, 2H, C_6H_4, J = 4.0 Hz), 7.78 (d, 2H, C_6H_4, J = 4.0 Hz), 8.49 (d, 1H, CONH, J = 4.0 Hz), 10.09 (s, 1H, 3-NH), 10.58 (s, 1H, 7-NH). Anal. ($C_{22}H_{25}N_5O_6\cdot 1.2H_2O$).

(*S*)-2-(4-(5-(2-Amino-4-oxo-4,7-dihydro-3*H*-pyrrolo[2,3-*d*]-pyrimidin-5-yl)pentyl)benzamido)pentanedioic Acid (9). Compound **9** was synthesized as described for **5** (yield 93%) as a blue powder. mp > 167 °C decomposed. R_f = 0.08 ($CHCl_3$/MeOH, 5:1). ^{1}H NMR (500 MHz, DMSO-d_6) δ 1.29−1.32 (m, 2H, CH_2), 1.58−1.62 (m, 4H, 2 CH_2), 1.92−2.00 (m, 1H, CH_2), 2.03−2.13 (m, 1H, CH_2), 2.34 (t, 2H, CH_2, J = 7.5 Hz), 2.53−2.55 (m, 2H, CH_2), 2.62 (t, 2H, CH_2, J = 7.5 Hz), 4.37−4.40 (m, 1H, CH), 5.94 (s, 2H, 2-NH_2), 6.31 (d, 1H, CH, J = 1.0 Hz), 7.28 (d, 2H, C_6H_4, J = 4.0 Hz), 7.78 (d,

2H, C_6H_4, J = 4.0 Hz), 8.50 (d, 1H, CONH, J = 4.0 Hz), 10.08 (s, 1H, 3-NH), 10.58 (s, 1H, 7-NH). Anal. ($C_{23}H_{27}N_5O_6 \cdot 1.0H_2O$).

(*S*)-2-(4-(6-(2-Amino-4-oxo-4,7-dihydro-3*H*-pyrrolo[2,3-*d*]-pyrimidin-5-yl)hexyl)benzamido)pentanedioic Acid (10). Compound **10** was synthesized as described for **5** (yield 93%) as a blue powder. mp > 178 °C decomposed. R_f = 0.10 ($CHCl_3$/MeOH, 5:1). ^{1}H NMR (500 MHz, DMSO-d_6) δ 1.27−1.32 (m, 4H, 2 CH_2), 1.53−1.62 (m, 4H, 2 CH_2), 1.92−2.00 (m, 1H, CH_2), 2.03−2.13 (m, 1H, CH_2), 2.34 (t, 2H, CH_2, J = 7.5 Hz), 2.52−2.54 (m, 2H, CH_2), 2.60 (t, 2H, CH_2, J = 7.5 Hz), 4.36−4.41 (m, 1H, CH), 5.94 (s, 2H, 2-NH_2), 6.31 (d, 1H, CH, J = 1.0 Hz), 7.28 (d, 2H, C_6H_4, J = 4.0 Hz), 7.78 (d, 2H, C_6H_4, J = 4.0 Hz), 8.50 (d, 1H, CONH, J = 4.0 Hz), 10.07 (s, 1H, 3-NH), 10.57 (s, 1H, 7-NH). Anal. ($C_{24}H_{29}N_5O_6 \cdot 1.77CH_3OH \cdot 0.1HCl$).

Molecular Modeling and Computational Studies. The X-ray crystal structures of human GARFTase at 1.98 Å resolution (PDB ID 1NJS)[35] and human AICARFTase at 2.55 Å resolution (PDB ID 1P4R)[36] were obtained from the Protein Data Bank. The GARFTase crystal structure contains human GARFTase complexed with the hydrolyzed form of 10-trifluoroacetyl-5,10-dideaza-acyclic-5,6,7,8-tetrahydrofolic acid (10-CF_3CO-DDACTHF), whereas the AICARFTase crystal structure contains human AICARFTase complexed with the sulfamido-bridged 5,8-dideazafolate analogue BW1540.

Docking studies were performed using LeadIT 1.3.[42] The protonation state of the proteins and the ligands were calculated using the default settings. Water molecules in the active site were permitted to rotate freely. The active site was defined by a sphere of 6.5 Å from the native ligand in the crystal structure. Ligands for docking were prepared using MOE 2010.10[43] and energy-minimized using the MMF94X forcefield to a constant of 0.05 kcal/mol. Triangle matching was used as the placement method, and the docked poses were scored using default settings. The docked poses were exported and visualized in MOE.

Molecules used for the docking experiments were constructed in MOE 2010.11 and minimized using the MMFF94x forcefield to a constant of 0.05 kcal/mol. To validate the docking software for docking the proposed compounds, the native ligands, 10-CF_3CO-DDACTHF for GARFTase and BW1540 for AICARFTase, were built using the molecule builder function in MOE, energy minimized, and docked, as described above. rmsd of the docked poses were calculated using an SVL code obtained from the MOE web site (www.chemcomp.com) and compared to the conformation of the crystal structure ligands.

The best docked pose for 10-CF_3CO-DDACTHF in the human GARFTase crystal structure had an rmsd of 1.0368 Å, and the best docked pose for BW1540 had an rmsd of 1.0995 Å in the AICARFTase crystal structure. Thus, LeadIT 1.3. was validated for our docking purposes in GARFTase and AICARFTase.

Reagents for Biological Studies. [3′,5′,7-^{3}H]MTX (20 Ci/mmol), [3′,5′,7,9-^{3}H] folic acid (25 Ci/mmol), and [^{14}C(U)]-glycine (87mCi/mmol) were purchased from Moravek Biochemicals (Brea, CA). Unlabeled folic acid was purchased from the Sigma Chemical Co. (St. Louis, MO). LCV ((6*R*,*S*)-5-formyl tetrahydrofolate) was provided by the Drug Development Branch, National Cancer Institute, Bethesda, MD. The sources of the classical antifolate drugs were as follows: MTX, Drug Development Branch, National Cancer Institute (Bethesda, MD); RTX (*N*-(5-(*N*-(3,4-dihydro-2-methyl-4-oxyquinazolin-6-ylmethyl)-*N*-methyl-amino]-2-thienoyl)-L-glutamic acid), AstraZeneca Pharmaceuticals (Maccesfield, Cheshire, England); LMTX (5,10-dideaza-5,6,7,8-tetrahydrofolate), Eli Lilly and Co. (Indianapolis, IN); and PMX (*N*-{4-(2-(2-amino-3,4-dihydro-4-oxo-7*H*-pyrrolo[2,3-*d*]pyrimidin-5-yl)ethyl)benzoyl}-L-glutamic acid) (Alimta) (LC Laboratories, Woburn, MA). Other chemicals were obtained from commercial sources in the highest available purity.

Cell Culture. MTXRIIOua^{R}2-4 (referred to as R2) is a RFC-, PCFT-, and FRα-null Chinese hamster ovary (CHO) cell line that was a gift from Dr. Wayne Flintoff (University of Western Ontario).[44] From this parental cell line, RFC, PCFT, and FRα were transfected to give rise to isogenic CHO cell lines designated PC43-10 (expresses human RFC but not PCFT or FRα), R2/PCFT4 (expresses PCFT), and RT16 (expresses FRα).[15−20,45] The CHO sublines were all maintained in α-minimal essential medium (α-MEM) supplemented with a 5% penicillin−streptomycin solution, 2 mM L-glutamate, and 10% heat-treated bovine calf serum (Invitrogen). Transfected cell lines were cultured in the presence of 1.5 mg/mL of G418. CHO cell lines were cultured prior to cell viability experiments in folate-free RPMI (FF-RPMI) (Invitrogen) with dialyzed fetal bovine serum (DFBS) (Invitrogen) supplemented with 5% penicillin-streptomycin and L-glutamate. FRα-expressing human KB nasopharyngeal carcinoma cells were continuously maintained in complete FF-RPMI with 10% fetal bovine serum, 5% penicillin−streptomycin, and L-glutamate.

Cell proliferation assays were performed exactly as previously described.[15−19] Cell lines were treated with a range of concentrations of standard or novel antifolates (0−1 μM), metformin (0−10 mM), or AICA (0−2 mM) in a 96-well plate in FF-RPMI complete with DFBS, 2 (RT-16, KB, IGROV1) or 25 nM (R2/PCFT4) LCV, penicillin−streptomycin, and L-glutamate over a 96 h incubation period at 37 °C with 5% CO_2. To confirm FRα-mediated drug uptake and growth inhibition, 200 nM folic acid was added to the incubations with drug. For proliferation assays with PC43-10 cells, cells were cultured in standard RPMI1640 with DFBS, penicillin−streptomycin, and L-glutamate for 96 h. To quantitate viable cells, media was removed and Cell Titer-blue fluorescent reagent (Promega) was added. Relative cell numbers were determined by relative fluorescence units measured with a fluorescence plate reader (Molecular Devices) at 590 nm emission and 560 nm excitation with Softmax Pro plate reader software. IC_{50} values, corresponding to the drug concentrations that resulted in 50% loss of cell growth, were calculated from dose−response curves using SigmaPlot (v.12) software.

To identify the targeted pathways/folate-dependent enzymes by the classic and novel pyrrolo[2,3-*d*]pyrimidine antifolates, proliferation assays were performed in the presence of adenosine (60 μM), thymidine (10 μM), or AICA hydrochloride (320 μM), and the results were compared to incubations performed in parallel without nucleoside/AICA or drug additions.

Colony-forming assays were performed with compound **8** to verify a cytotoxic (as opposed to cytostatic) response. KB cells (~500 cells) were plated in 60 mm dishes in FF-RPMI/DFBS supplemented with 2 nM LCV for a 24 h incubation period at 37 °C in the presence of 5% CO_2. Concentrations from 0 to 10 μM of compound **8** were added to media for an additional 24 h, after which the media was aspirated and replaced with complete FF-RPMI supplemented with 2 nM LCV for 8−10 days. To visualize colonies, the cells were washed (2×) with room temperature Dulbecco's phosphate-buffered saline (PBS) (Sigma) followed by a wash of 5% trichloroactetic acid (TCA). The TCA was removed, and 10 mM borate buffer (pH 8.8) was added followed by a 30 min incubation with 1% methylene blue in borate buffer at room temperature. The cells were washed three times with borate buffer, and the stained colonies were counted.

Competitive MTX Transport Assays. To determine if novel antifolates bound to RFC, reflecting membrane transport by this mechanism, competition with [^{3}H]MTX for cellular uptake was measured in RFC-expressing PC43-10 CHO cells.[15,18] PC43-10 cells (~1.5 × 10^6 cells) were seeded in 60 mm dishes. After 48 h, cells were washed with PBS and uptake of [^{3}H]MTX (0.5 μM) was measured in Hank's balanced salts solution for 2 min at 37 °C. Ice-cold PBS was used to quench the reactions. Cells were washed with ice-cold PBS (3×) and then solubilized with 0.5 N NaOH. The cellular homogenates were assayed for radioactivity with a liquid scintillation counter, and protein concentrations were measured with Folin-phenol reagent.[46] Levels of drug uptake were expressed as picomoles per milligram of cell protein.

FRα Binding Assay. To determine the binding affinity of novel antifolates to FRα, FRα-expressing RT16 CHO cells (~1.5 x10^6 cells) were seeded in a monolayer with complete α-MEM media. Cells were washed with ice-cold PBS followed by ice-cold acetate buffer (10 mM sodium acetate, 150 mM NaCl, pH 3.5) to release FRα-bound folates and then neutralized with ice-cold HEPES-buffered saline (HBS) (20 mM HEPES, 140 mM NaCl, 5 mM KCl, 2 mM $MgCl_2$, 5 mM glucose, pH 7.4). Cells were then incubated at 0 °C for 15 min in a cocktail

containing [3′,5′,7′,9-^{3}H]folic acid in the absence or presence of unlabled folic acid or novel antifolate compounds over a range of concentrations. Cells were washed with ice-cold HBS and solubilized with 0.5 N NaOH. The cell homogenates were collected and analyzed for radioactivity using a liquid scintillation counter. Protein concentrations were measured with Folin-phenol reagent.[46] Bound [^{3}H]folic acid was expressed as picomoles per milligram of protein. Using SigmaPlot (v. 12) software, dose−response curves were created, and IC_{50}'s were calculated. Relative binding affinities were calculated as the inverse molar ratios of unlabeled ligands required to inhibit [^{3}H]folic acid by 50%, as determined graphically with GraphPad (v. 6.0) software. By definition, the relative affinity of folic acid is 1.

HPLC Detection of ATP. Intracellular ATP concentrations were determined using nucleotide extractions and an HPLC method exactly as previously described.[20,33] Briefly, KB cells were seeded in a T75 flask with FF-RPMI with 10% DFBS, 5% penicillin−streptomycin, 2 mM L-glutamine, and 2 nM LCV. Cells were treated with 1 μM of PMX or compounds **2** or **8** for 24 h. After the incubations, cells were trypsinized and washed with cold PBS. Nucleotide pools were fractionated by reversed-phase HPLC on a C18 column for determination of ATP pools.[20]

Apoptosis and Cell Cycle Analyses. Apoptosis and cell cycle analyses were performed through the Microscopy, Imaging, and Cytometry Resources Core of the Karmanos Cancer Institute. KB cells were treated with 1 μM of PMX or compounds **2** or **8** for 48 and 96 h in FF-RPMI media complete with 10% DFBS, 5% penicillin−streptomycin, and 2 nM LCV. Cells were harvested by trypsinization and washed with cold PBS. Cells were equally divided into two pools and either assayed for cell cycle distribution or for apoptosis by flow cytometry using the BD FACSCanto II flow cytometer operated with BD FACSDiva software (v6.0) (BD Biosciences). For cell cycle analysis, cells were fixed with ice-cold ethanol (added dropwise) and then stained with 50 μg/mL of PI and 100 μg/mL of RNase (type I-A) (Sigma) in PBS for at least 20 min at room temperature in the dark prior to analysis by flow cytometry, with a minimum of 10 000 events (cells) analyzed. Apoptosis was measured using the annexin V-FITC/7-AAD kit, as specified by the manufacturer (Beckman Coulter), with a minimum of 20 000 events (cells) analyzed for early apoptosis (annexin-V-FITC^{high}/7-AAD^{low}; Q3) and late apoptosis/necrosis (annexin-V-FITC^{high}/7-AAD^{high}; Q2)]; viable cells are shown in Q4 (annexin-V-FITC^{low}/7-AAD^{low}). All data were analyzed with FlowJo (v7.6.1) software (Tree Star, Inc.). The Watson Pragmatic model was used to analyze cell cycle distributions of G_1/G_o-, S-, and G_2/M-phase cells and to estimate the sub-G_1 (late apoptotic cell) fraction.

In Situ GARFTase Inhibition Assays. To measure the extent of intracellular GARFTase inhibition in the presence of antifolate inhibitors, we examined the metabolic incorporation of [^{14}C(U)]-glycine into [^{14}C]formyl GAR in the presence of azaserine.[15−20,32] KB cells were seeded in complete media (above) and allowed to adhere to the substratum for 24 h. Cells were then washed with FF-RPMI, L-glutamine-free, with 10% DFBS, 5% penicillin−streptomycin, and 2 nM LCV. Cells were incubated at 37 °C with 5% CO_2 for 1 h with folate- and L-glutamine-depleted media containing 2 nM LCV with PMX or with compounds **2** or **8** over a range of concentrations. Control cells were treated with DMSO of equal volume. Azaserine (4 μM final concentration) was added to the cells and allowed to incubate for 30 min. This was followed by the addition of L-glutamine (2 mM) and [^{14}C(U)]glycine (final specific activity 0.1 mCi/L). Cells were incubated 16 h. Cells were washed with ice-cold PBS, trypsinized, and collected. Cells were treated with 5% TCA at 0 °C. Samples were centrifuged (4 °C, 14 000 rpm), and the protein precipitants were solubilized with 0.5 N NaOH for quantitation of protein concentrations with the Folin-phenol protein method.[46] The TCA supernatants were extracted with cold ether. After evaporation of ether, the remaining aqueous layer was gravity filtered through a 1 cm chromatography column (Biorad) of AG1 × 8 (chloride form). The columns were washed with 10 mL of 0.5 N formic acid followed by 4 N formic acid (10 mL) and finally eluted with 8 mL of 1 N HCL collected in eight fractions. The eluate was measured for radioactivity, and the percentages of radioactivity in the [^{14}C]formyl GAR and nonspecific [^{14}C]fractions. The results were calculated as pmol [^{14}C]formyl GAR/mg protein. Data were graphed using SigmaPlot (v.12), and the IC_{50}'s were calculated for the antifolate-treated samples compared to the untreated controls.

HPLC Detection of ZMP Pools. Methods for detecting ZMP in KB cells treated with the antifolate drugs were based on those described by Rascanelli et al.[22,23] Briefly, KB cells were treated with PMX or compound **8** for 48 h in FF-RPMI with 10% DFBS, 5% penicillin−streptomycin, 2 mM L-glutamine, and 2 nM LCV. Cells were washed with PBS and treated with ice-cold 5% TCA, and the precipitated proteins were collected by centrifugation (1600 rpm, 10 min). The soluble fractions were extracted with ether (2×) and fractionated by ion-exchange HPLC on a SAX 250 × 2 mm column (Phenomenex) with a linear gradient from 5 mM $NH_4H_2PO_4$ (pH 2.8) to 750 mM $NH_4H_2PO_4$ (pH 3.9) over 25 min at a flow rate of 0.2 mL/min. Absorbance was monitored at 280 nm, and the intracellular ZMP concentrations were established by fitting the peak absorbances to a standard curve with commercial ZMP. AraCMP was used as an internal control.

Western Blot Analysis. KB cells were treated for 48 h with PMX or with compound **8** in the presence of thymidine (10 μM). Controls include vehicle control (water or DMS0 as appropriate; results were identical) or known activators of AMPK, including metformin (10 mM), AICA (1 mM), or AICA ribonucleoside (AICAR) (1 mM). Cells were washed, suspended in 10 mM Tris-HCl (pH 7.0) plus proteolytic and phosphatase inhibitors (Roche Applied Science), and disrupted by sonication. Samples were centrifuged (14 000 rpm, 10 min), and 90 μg of protein was fractionated by SDS polyacrylamide gel electrophoresis on Laemmli gradient gels (4−20%).[47] Proteins were electrotransferred to polyvinylidene difluoride membranes (Pierce).[48] Detection of immunoreactive AMPK was with rabbit total and phospho-AMPK antibodies (Cell Signaling) and an IRDye800-conjugated secondary anti-rabbit antibody (LI-COR, Lincoln, NE) using an Odyssey infrared imaging system (LI-COR). β-actin was detected with an anti-β-actin mouse antibody (Sigma) and an IRDye800-conjugated secondary anti-mouse antibody (LI-COR).

■ ASSOCIATED CONTENT

Ⓢ Supporting Information

Cell cycle distributions and apoptosis in KB cells treated with pemetrexed (PMX) or compounds **2** or **8** for 48 h, inhibition of KB cell proliferation with the AMPK activator metformin, and elemental analyses. This material is available free of charge via the Internet at http://pubs.acs.org.

■ AUTHOR INFORMATION

Corresponding Authors

*Phone: 313-578-4280; Fax: 313-578-4287; E-mail: matherly@karmanos.org (L.H.M.).

*Phone: 412-396-6070; Fax: 412-396-5593; E-mail: gangjee@duq.edu (A.G.).

Present Address

[#]Center for Drug Discovery and Translational Research, Beth Israel Deaconess Medical Center, Harvard Medical School, Boston, Massachusetts 02215, United States.

Author Contributions

[⊥]These authors contributed equally to this work

Notes

The authors declare no competing financial interest.

■ ACKNOWLEDGMENTS

This work was supported in part by grants from the National Institutes of Health, National Cancer Institute R01 CA152316 (L.H.M. and A.G.), R01 CA166711 (A.G. and L.H.M.), and R01 CA53535 (L.H.M.), and the Duquesne University Adrian

Van Kaam Chair in Scholarly Excellence (A.G.). Ms. Mitchell-Ryan was supported by T32 CA009531 (L.H.M.) and F31 CA165853 (S.M.R.). We thank Dr. Mark Stout for his assistance with the HPLC analyses of cellular ZMP. The Microscopy, Imaging and Cytometry Resources Core is supported, in part, by NIH Center Grant P30 CA22453 (to the Barbara Ann Karmanos Cancer Institute) and the Perinatology Research Branch of the NICHD, NIH, Wayne State University.

■ ABBREVIATIONS USED

IC_{50}, 50% inhibitory concentration; AAD, amino actinomycin D; α-MEM, α-minimal essential medium; AICA, 5-amino-imidazole-4-carboxamide; AICAR, 5-aminoimidazole-4-carbox-amide ribonucleoside; AICARFTase, 5-aminoimidazole-4-car-boxamide ribonucleotide formyltransferase; AMPK, AMP-activated protein kinase; CHO, Chinese hamster ovary; DFBS, dialyzed fetal bovine serum; DHFR, dihydrofolate reductase; FITC, fluorescein isothiocyanate; FF-RPMI, folate-free RPMI1640; FR, folate receptor; GAR, glycinamide ribonucleotide; GARFTase, glycinamide ribonucleotide formyl-transferase; HBS, HEPES-buffered saline; LCV, leucovorin; LMTX, lometrexol; MTX, methotrexate; PMX, pemetrexed; PBS, phosphate-buffered saline; PCFT, proton-coupled folate transporter; PI, propidium iodine; RTX, raltiterxed; RFC, reduced folate carrier; SAR, structure−activity relationship; TCA, trichloroacetic acid; TS, thymidylate synthase; ZMP, 5-aminoimidazole-4-carboxamide ribonucleotide

■ REFERENCES

(1) Visentin, M.; Zhao, R.; Goldman, I. D. The Antifolates. *Hematol. Oncol. Clin. North Am.* **2012**, *26*, 629−648.

(2) Gonen, N.; Assaraf, Y. G. Antifolates in Cancer Therapy: Structure, Activity and Mechanisms of Drug Resistance. *Drug Resist. Updates* **2012**, *15*, 183−210.

(3) Mendelsohn, L. G.; Worzalla, J. F.; Walling, J. M. Preclinical and Clinical Evaluation of the Glycinamide Ribonucleotide Formyltransferase Inhibitors Lometrexol and LY309887. In *Anticancer Drug Development Guide: Antifolate Drugs in Cancer Therapy*; Jackman, A. L., Ed.; Humana Press, Inc.: Totowa, NJ, 1999; pp 261−280.

(4) Budman, D. R.; Johnson, R.; Barile, B.; Bowsher, R. R.; Vinciguerra, V.; Allen, S. L.; Kolitz, J.; Ernest, C. S., II; Kreis, W.; Zervos, P.; Walling, J. Phase I and Pharmacokinetic Study of LY309887: A Specific Inhibitor of Purine Biosynthesis. *Cancer Chemother. Pharmacol.* **2001**, *47*, 525−553.

(5) Boritzki, T. J.; Zhang, C.; Bartlett, C. A.; Jackson, R. C. AG2034 a GARFTASE Inhibitor with Selective Cytotoxicity to Cells That Lack a G1 Checkpoint. In *Anticancer Drug Development Guide: Antifolate Drugs in Cancer Therapy*; Jackman, A. L., Ed.; Humana Press Inc.: Totowa, NJ, 1999; pp 281− 292.

(6) Ray, M. S.; Muggia, F. M.; Leichman, C. G.; Grunberg, S. M.; Nelson, R. L.; Dyke, R. W.; Moran, R. G. Phase I Study of (6R)-5,10-Dideazatetrahydrofolate: A Folate Antimetabolite Inhibitory to De Novo Purine Synthesis. *J. Natl. Cancer Inst.* **1993**, *85*, 1154−1159.

(7) Bissett, D.; McLeod, H. L.; Sheedy, B.; Collier, M.; Pithavala, Y.; Paradiso, L.; Pitsiladis, M.; Cassidy, J. Phase I Dose-Escalation and Pharmacokinetic Study of a Novel Folate Analogue AG2034. *Br. J. Cancer* **2001**, *84*, 308−312.

(8) Matherly, L. H.; Hou, Z.; Deng, Y. Human Reduced Folate Carrier: Translation of Basic Biology to Cancer Etiology and Therapy. *Cancer Metastasis Rev.* **2007**, *26*, 111−128.

(9) Elnakat, H.; Ratnam, M. Distribution, Functionality and Gene Regulation of Folate Receptor Isoforms: Implications in Targeted Therapy. *Adv. Drug Delivery Rev.* **2004**, *56*, 1067−1084.

(10) Zhao, R.; Goldman, I. D. The Molecular Identity and Characterization of a Proton-Coupled Folate Transporter−PCFT; Biological Ramifications and Impact on the Activity of Pemetrexed. *Cancer Metastasis Rev.* **2007**, *26*, 129−139.

(11) Kugel Desmoulin, S.; Hou, Z.; Gangjee, A.; Matherly, L. H. The Human Proton-Coupled Folate Transporter: Biology and Therapeutic Applications to Cancer. *Cancer Biol. Ther.* **2012**, *13*, 1−19.

(12) Kamen, B. A.; Smith, A. K. Farletuzumab, an Anti-Folate Receptor α Antibody, Does Not Block Binding of Folate or Anti-Folates to Receptor nor Does It Alter the Potency of Anti-Folates In Vitro. *Cancer Chemother. Pharmacol.* **2012**, *70*, 113−120.

(13) Xia, W.; Low, P. S. Folate-Targeted Therapies for Cancer. *J. Med. Chem.* **2010**, *53*, 6811−6824.

(14) Gibbs, D. D.; Theti, D. S.; Wood, N.; Green, M.; Raynaud, F.; Valenti, M.; Forster, M. D.; Mitchell, F.; Bavetsias, V.; Henderson, E.; Jackman, A. L. BGC 945, a Novel Tumor-selective Thymidylate Synthase Inhibitor Targeted to Alpha-Folate Receptor-Overexpressing Tumors. *Cancer Res.* **2005**, *65*, 11721−11728.

(15) Deng, Y.; Wang, Y.; Cherian, C.; Hou, Z.; Buck, S. A.; Matherly, L. H.; Gangjee, A. Synthesis and Discovery of High Affinity Folate Receptor-Specific Glycinamide Ribonucleotide Formyltransferase Inhibitors with Antitumor Activity. *J. Med. Chem.* **2008**, *51*, 5052−5063.

(16) Deng, Y.; Zhou, X.; Desmoulin, S. K.; Matherly, L. H.; Gangjee, A. Synthesis and Biological Activity of a Novel Series of 6-Substituted Thieno[2,3-*d*]pyrimidine Antifolate Inhibitors of Purine Biosynthesis with Selectivity for High Affinity Folate Receptors over the Reduced Folate Carrier and Proton-Coupled Folate Transporter for Cellular Entry. *J. Med. Chem.* **2009**, *52*, 2940−2951.

(17) Wang, L.; Cherian, C.; Desmoulin, S. K.; Polin, L.; Deng, Y.; Wu, J.; Hou, Z.; White, K.; Kushner, J.; Matherly, L. H.; Gangjee, A. Synthesis and Antitumor Activity of a Novel Series of 6-Substituted Pyrrolo[2,3-*d*]pyrimidine Thienoyl Antifolate Inhibitors of Purine Biosynthesis with Selectivity for High Affinity Folate Receptors and the Proton-Coupled Folate Transporter over the Reduced Folate Carrier for Cellular Entry. *J. Med. Chem.* **2010**, *53*, 1301−1318.

(18) Wang, L.; Desmoulin, S. K.; Matherly, L. H.; Gangjee, A. Synthesis, Biological, and Antitumor Activity of a Highly Potent 6-Substituted Pyrrolo[2,3-*d*] pyrimidine Thienoyl Antifolate Inhibitor with Proton-Coupled Folate Transporter and Folate Receptor Selectivity over the Reduced Folate Carrier that Inhibits β-Glycinamide Ribonucleotide Formyltransferase. *J. Med. Chem.* **2011**, *54*, 7150−7164.

(19) Wang, L.; Cherian, C.; Desmoulin, S. K.; Matherly, L. H.; Gangjee, A. Synthesis and Biological Activity of 6-Substituted Pyrrolo[2,3-*d*]pyrimidine Thienoyl Regioisomers as Inhibitors of De Novo Purine Biosynthesis with Selectivity for Cellular Uptake by High Affinity Folate Receptors and the Proton-Coupled Folate Transporter over the Reduced Folate Carrier. *J. Med. Chem.* **2012**, *55*, 1758−1770.

(20) Desmoulin, S. K.; Wang, Y.; Gangjee, A.; Matherly, L. H. Targeting the Proton-Coupled Folate Transporter for Selective Delivery of 6-Substituted Pyrrolo[2,3-*d*]pyrimidine Antifolate Inhibitors of De Novo Purine Biosynthesis in the Chemotherapy of Solid Tumors. *Mol. Pharmacol.* **2010**, *78*, 577−587.

(21) Chattopadhyay, S.; Moran, R. G.; Goldman, I. D. Pemetrexed: Biochemical and Cellular Pharmacology, Mechanisms, and Clinical Applications. *Mol. Cancer Ther.* **2007**, *6*, 404−417.

(22) Racanelli, A. C.; Rothbart, S. B.; Heyer, C. L.; Moran, R. G. Therapeutics by Cytotoxic Metabolite Accumulation: Pemetrexed Causes ZMP Accumulation, AMPK Activation, and Mammalian Target of Rapamycin Inhibition. *Cancer Res.* **2009**, *69*, 5467−5474.

(23) Rothbart, S. B.; Racanelli, A. C.; Moran, R. G. Pemetrexed Indirectly Activates the Metabolic Kinase AMPK in Human Carcinomas. *Cancer Res.* **2010**, *70*, 10299−10309.

(24) Mihaylova, M. M.; Shaw, R. J. The AMPK Signalling Pathway Coordinates Cell Growth, Autophagy and Metabolism. *Nat. Cell Biol.* **2011**, *13*, 1016−1023.

(25) Gwinn, D. M.; Shackelford, D. B.; Egan, D. F.; Mihaylova, M. M.; Mery, A.; Vasquez, D. S.; Turk, B. E.; Shaw, R. J. AMPK Phosphorylation of Raptor Mediates a Metabolic Checkpoint. *Mol. Cell* **2008**, *30*, 214−226.

(26) Inoki, K.; Zhu, T.; Guan, K. L. TSC2 Mediates Cellular Energy Response to Control Cell Growth and Survival. *Cell* **2003**, *115*, 577−590.
(27) Ma, X. M.; Blenis, J. Molecular Mechanisms of mTOR-Mediated Translational Control. *Nat. Rev. Mol. Cell Biol.* **2009**, *10*, 307−318.
(28) Barnett, C. J.; Wilson, T. M.; Kobierski, M. E. A Practical Synthesis of Multitargeted Antifolate LY231514. *Org. Process Res. Dev.* **1999**, *3*, 184−188.
(29) Aso, K.; Imai, Y.; Yukishige, K.; Ootsu, K.; Akimoto, H. Pyrrolo[2,3-*d*]pyrimidine Thymidylate Synthase Inhibitors: Design and Synthesis of One-Carbon Bridge Derivatives. *Chem. Pharm. Bull.* **2001**, *49*, 1280−1287.
(30) Larock, R. C.; Leung, W. Y.; Stolzdunn, S. Synthesis of Aryl-Substituted Aldehydes and Ketones via Palladium-Catalyzed Coupling of Aryl Halides and Non-Allylic Unsaturated Alcohols. *Tetrahedron Lett.* **1989**, *30*, 6629−6632.
(31) Bloch, R. 5,5-Dibromo-2,2-dimethyl-4,6-dioxo-1,3-dioxane − New Brominating Agent for Saturated and Alpha,Beta-Unsaturated Carbonyl-Compounds. *Synthesis* **1978**, 140−142.
(32) Beardsley, G. P.; Moroson, B. A.; Taylor, E. C.; Moran, R. G. A New Antimetabolite, 5,10-Dideaza-5,6,7,8-tetrahydrofolate is a Potent Inhibitor of De Novo Purine Synthesis. *J. Biol. Chem.* **1989**, *264*, 328−333.
(33) Huang, D.; Zhang, Y.; Chen, X. Analysis of Intracellular Nucleoside Triphosphate Levels in Normal and Tumor Cell Lines by High-Performance Liquid Chromatography. *J. Chromatogr., B: Anal. Technol. Biomed. Life Sci.* **2003**, *784*, 101−109.
(34) Brown, J. M.; Attardi, L. D. The Role of Apoptosis in Cancer Development and Treatment Response. *Nat. Rev. Cancer* **2005**, *5*, 31−37.
(35) Cheong, C.-G.; Wolan, D. W.; Greasley, S. E.; Horton, P. A.; Beardsley, G. P.; Wilson, I. A. Crystal Structures of Human Bifunctional Enzyme Aminoimidazole-4-carboxamide Ribonucleotide Transformylase/IMP Cyclohydrolase in Complex with Potent Sulfonyl-Containing Antifolates. *J. Biol. Chem.* **2004**, *279*, 18034−18045.
(36) Zhang, Y.; Desharnais, J.; Marsilje, T. H.; Li, C.; Hedrick, M. P.; Gooljarsingh, L. T.; Tavassoli, A.; Benkovic, S. J.; Olson, A. J.; Boger, D. L.; Wilson, I. A. Rational Design, Synthesis, Evaluation, and Crystal Structure of a Potent Inhibitor of Human GAR Tfase: 10-(Trifluoroacetyl)-5,10-dideazaacyclic-5,6,7,8-tetrahydrofolic Acid. *Biochemistry.* **2003**, *42*, 6043−6056.
(37) Hazarika, M.; White, R. M.; Johnson, J. R.; Pazdur, R. FDA Drug Approval Summaries: Pemetrexed (Alimta). *Oncologist* **2004**, *9*, 482−488.
(38) Thompson, C. A. FDA Approves Pralatrexate for Treatment of Rare Lymphoma. *Am. J. Health-Syst. Pharm.* **2009**, *66*, 1890.
(39) Chen, C.; Ke, J.; Zhou, X. E.; Yi, W.; Brunzelle, J. S.; Li, J.; Yong, E. L.; Xu, H. E.; Melcher, K. Structural Basis for Molecular Recognition of Folic Acid by Folate Receptors. *Nature* **2013**, *500*, 486−489.
(40) Wibowo, A. S.; Singh, M.; Reeder, K. M.; Carter, J. J.; Kovach, A. R.; Meng, W.; Ratnam, M.; Zhang, F.; Dann, C. E., 3rd. Structures of Human Folate Receptors Reveal Biological Trafficking States and Diversity in Folate and Antifolate Recognition. *Proc. Natl. Acad. Sci. U.S.A.* **2013**, *110*, 15180−15188.
(41) Taylor, E. C.; Kuhnt, D.; Shih, C.; Rinzel, S. M.; Grindey, G. B.; Barredo, J.; Jannatipour, M.; Moran, R. G. A Dideazatetrahydrofolate Analog Lacking a Chiral Center at C-6: *N*-[4-[2-(2-Amino-3,4-dihydro-4-oxo-7*H*-pyrrolo[2,3-*d*]pyrimidin-5yl)ethyl[benzoyl]-L-glutamic Acid Is an Inhibitor of Thymidylate Synthase. *J. Med. Chem.* **1992**, *35*, 4450−4454.
(42) *LeadIT*, version 1.3; BioSolveIT GmbH: Sankt Augustin, Germany, 2011.
(43) *MOE*, 2010.10; Chemical Computing Group: Montreal, Quebec, Canada.
(44) Flintoff, W. F.; Davidson, S. V.; Siminovitch, L. Isolation and Partial Characterization of Three Methotrexate-Resistant Phenotypes from Chinese Hamster Ovary Cells. *Somatic Cell Genet.* **1976**, *2*, 245−261.
(45) Wong, S. C.; Proefke, S. A.; Bhushan, A.; Matherly, L. H. Isolation of Human cDNAs That Restore Methotrexate Sensitivity and Reduced Folate Carrier Activity in Methotrexate Transport-Defective Chinese Hamster Ovary Cells. *J. Biol. Chem.* **1995**, *270*, 17468−17475.
(46) Lowry, O. H.; Rosebrough, N. J.; Farr, A. L.; Randall, R. J. Protein Measurement with the Folin Phenol Reagent. *J. Biol. Chem.* **1951**, *193*, 265−275.
(47) Laemmli, U. K. Cleavage of Structural Proteins During the Assembly of the Head of Bacteriophage T4. *Nature* **1970**, *227*, 680−685.
(48) Matsudaira, P. Sequence from Picomole Quantities of Proteins Electroblotted onto Polyvinylidene Difluoride Membranes. *J. Biol. Chem.* **1989**, *262*, 10035−10038.